DIRECT MEASUREMENTS OF ELECTRON ENERGY
DISTRIBUTIONS IN THE DAYTIME IONOSPHERE

BY

PHILIP T. HUANG

UNIVERSITY OF MARYLAND
DEPARTMENT OF PHYSICS AND ASTRONOMY
COLLEGE PARK, MARYLAND
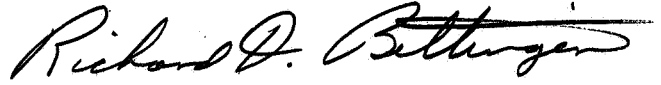
FEBRUARY 1969

APPROVAL SHEET

Title of Thesis: Direct Measurements of Electron Energy
                    Distributions in the Daytime Ionosphere

Name of Candidate: Philip T. Huang
                    Doctor of Philosophy, 1969

Thesis and Abstract Approved:

Richard T. Bettinger
Assistant Professor of Physics
Department of Physics and Astronomy

Date Approved: 4/21/69

VITA

Name: Philip T. Huang

Permanent Address: 6002 Springhill Drive, Greenbelt, Maryland

Degree and Date to be conferred: Doctor of Philosophy, 1969

Date of Birth: April 2, 1938

Place of Birth: Peking, China

Secondary Education: Forest Hills High School, New York, New York, 1956

Collegiate Institutions Attended	Dates	Degree	Date of Degree
Massachusetts Institute of Technology, Cambridge, Massachusetts	1956-1961	B.S.	1961
University of Maryland, College Park, Maryland	1961-1969	Ph.D.	1969

Major: Physics

Minor: Astronomy

Publications: "Direct Probe Measurements in the Auroral Ionosphere," with R. T. Bettinger, University of Maryland, Department of Physics and Astronomy, Final Report on AFCRL Contract AF 19(628)2792, No. AFCRL 66-825, (1966).

"Langmuir Probes Employing Large Accelerating Potentials in the Ionosphere," AGU Transactions, 48 (1), 86 (March, 1967).

"Measurements on the Energy Distributions of Ionospheric Electrons," AGU Transactions, 49 (1), 148 (March, 1968)

Positions Held: Research Assistant, Department of Physics and Astronomy, University of Maryland, 1963 - Present

Teaching Assistant, Department of Physics and Astronomy, University of Maryland, 1963 Spring Semester

ABSTRACT

Title of Thesis: Direct Measurements of Electron Energy Distributions
                   in the Daytime Ionosphere

Philip T. Huang, Doctor of Philosophy, 1969

Thesis directed by: R. T. Bettinger, Assistant Professor of Physics

The energy distributions of electrons in the ionospheric plasma

have been obtained for the energy interval of 0 - 15 ev, from the

utilization of a pulse probe operated in the DC mode. The experiments

were conducted aboard four sounding rockets (NASA 14.164, 18.12, 14.298,

and 18.30), launched from Wallops Island, Virginia into normal daytime

ionospheres.

The observed retarded current-voltage characteristics indicate the

existence of two distinct distributions in this energy range, the

thermal distribution and a secondary distribution extending to

approximately 8 ev at the higher altitudes, with characteristic

temperatures of $\sim$ 1.5 to 2.5 x 10^3 $^{\circ}K$ and 1 to 3 x 10^4 $^{\circ}K$, respectively.

Both temperatures are observed to increase with increasing altitudes

in the region between $\sim$ 120 and 240 km.

The retarded probe currents corresponding to these two distributions

are exponential functions of the retarding probe potential. No valleys

or humps were observed to exist in the secondary energy distribution

function. The concentration of secondary electrons has the approximate

values of 150 - 200 electrons/cm^3 between $\sim$ 150 and 240 km.

A high energy electron component (E $\gtrsim$ 15 ev), in the ambient plasma,

was observed to have contributed to the total probe current. The retarded probe current from this distribution appears as a linear function of the retarding probe potential. Analysis of the magnitudes and the slopes of the measured current indicate characteristic energies of $\sim$ 26 ev, with a concentration between 5 - 14 electrons/cm^3, the latter increasing with increasing altitudes.

DIRECT MEASUREMENTS OF ELECTRON

ENERGY DISTRIBUTIONS IN THE DAYTIME IONOSPHERE

by

Philip T. Huang

February 1969

ACKNOWLEDGMENTS

My deep appreciation to Dr. Richard T. Bettinger for the direction and inspiration that he has given me throughout my graduate studies. The success of this research project can be directly attributed to his pioneering work in this field.

For their contributions to the design and construction of the payload instrumentation, I wish to thank Dean Jordan, Elwood Barnes, and Milton Grimsley.

I am indebted to Jerome Bohse for his help in the data processing and the many fruitful discussions we have had during our association. I wish to thank my brother, Frank, for his help with the computer programs used in the data analysis.

For her patience and dedication that she has shown me for these many years, I am deeply grateful to my wife, Esther.

I want to thank Mrs. Janis Kinsman for the gracious manner in which she has typed and assembled this thesis.

TABLE OF CONTENTS

TABLE OF CONTENTS
(Continued)

LIST OF TABLES

LIST OF FIGURES

CHAPTER I

INTRODUCTION

The ionosphere is a region of ionized gases consisting of electrons and singly charged ions, starting at approximately 50 km above the earth's surface. The subject of production and loss mechanisms, as well as the dynamics of the plasma particles have up to the present time occupied the center stage in the field of ionospheric studies.

The global network of ground based ionospheric sounders (ionosondes) has provided the bulk of the present-day knowledge concerning the altitude, geographic and time variations of the free electrons present in the lower regions of the ionosphere. The commonly accepted classification scheme which divides the lower ionosphere into various regions (the D, E, and F given in the order of ascending height) is based on the observed altitude profile of the electron concentration as determined by the reflection of radio waves from the bottomside sounder.

The ionization of the neutral atmosphere produced by cosmic rays is believed to occur below approximately 70 km and this region has been called the C region. Above approximately 300 km, where the peak of the electron concentration is usually observed, the density profile for the electrons can no longer be obtained from the ground based ionosondes. This region has been sometimes referred to as the topside ionosphere and has received a great deal of attention from recent experiments conducted aboard both satellites and sounding rockets. The Canadian satellites, Alouette I and II, for instance, conducted soundings from

the topside above the region of peak density using similar techniques as those employed in the bottomside soundings.

The major source of the ionization that occurs in the D, E, and F regions of the ionosphere is currently attributed to the incident solar radiation of wavelengths less than approximately 2400 $\overset{o}{A}$. The incident intensities corresponding to some of these ionizing wavelengths depend very strongly on solar activity. As a result, we find that various ionospheric parameters such as temperature, density, and composition experience a strong degree of solar influence.

For example, in the D region, which is commonly located between approximately 70 and 85 km, the origin of the observed ionization is believed to be H Lyman α (1215.7 $\overset{o}{A}$) radiation during quiet solar conditions. However, during a solar flare the large increases of x-rays in the 2 to 8 $\overset{o}{A}$ wavelength interval may become the major source of the enhanced D region ionization (Nicolet and Aiken, 1960; Bourdeau, 1963; Aiken and Bauer, 1965).

The altitude range between approximately 85 and 150 km has often been called the E region and above approximately 150 km, the F region. Extreme ultraviolet radiation (both line and continuum) and the x-rays in the vicinity of 30 $\overset{o}{A}$ are usually considered as the major sources of the ionization in the E region. The extreme ultraviolet solar radiations in the wavelength interval of 300 - 800 $\overset{o}{A}$ are believed to cause the formation of the F region.

Ideal, quiet ionospheric conditions are to some degree rare phenomena when one is confronted by the various sporadic and anomalous variations in the electron density. Even within the framework of

analyzing a so-called "normal," quiet mid-latitude ionosphere, there are many problems lacking satisfactory explanations. For instance, consider the fact that both the E and F regions display the presence of substantial nighttime ionizations despite presumably the turning off of the photoionization source and the relatively short recombination time constants, particularly in the E region.

The photoionization that occurs in the daytime ionosphere is only the beginning of a rather complex chain of events leading to the eventual heating of the neutral atmosphere; the details of which are not at all well understood at the present time. The equilibrium electron energy distribution not only reflects the complex nature of the ionizing solar radiation and its interaction with the neutral atmosphere, but upon the interaction of the photoelectrons with the existing medium. The primary electrons, whatever might be their source, may produce additional ionization or excitation of the particles they encounter. In this dissertation we shall be primarily concerned with the experimental determination of the equilibrium electron energy distributions in the energy range of 0 - 15 ev. For the electrons in this energy range, impact ionizations are essentially negligible in terms of energy loss, and excitations of neutral atoms, ions, and the ambient electron gas represent the major energy sinks in terms of particle interactions.

The utilization of sounding rockets and satellites for conducting ionospheric research has brought forth a wealth of new information to this field, together with the initiation of many new problems. The special advantages of being in a position to make direct measurements also bring forth demands for higher instrument reliability and

considerations of the interactions between the vehicle platform and the space environment which may seriously distort the data collected. This paper will present results gathered from one of a program of four rocket experiments launched from Wallops Island, Virginia. Each of the four payloads had borne a full complement of probes into generally quiet daytime ionospheres. A compendium of these four rocket experiments is provided in Table 1.1.

The primary objectives of these experiments were to: (1) measure the electron concentration and energy distribution with a recently developed pulse probe, (2) measure electron and ion parameters with the conventional Langmuir probe, and in particular investigate the use of wing-slope techniques, (3) examine the vehicle to plasma potential measurements from the thermal equalization probes (Bettinger, 1964), and (4) compare the electron energy distribution measurements of the pulse probe with that of the retarding potential analyzers. The selection of these experiments under one payload configuration lends itself readily for cross referencing and investigation of the relative capabilities of the various probes. We shall devote most of our attention to the analysis of the pulse probe data.

A method for determining the velocity distribution of the charged particles in an isotropic plasma by taking the second derivative of the particle current to a probe surface with respect to its retarding potential was first proposed by Druyvesteyn (1930). It is applicable to both charged species, electrons and ions, and in the case of an anisotropic velocity distribution, the relationship can only be utilized for a spherical probe. With standard operational

TABLE 1.1

RECENT SOUNDING ROCKET EXPERIMENTS CONDUCTED BY THE ATMOSPHERIC PHYSICS
GROUP (U. OF MARYLAND) FROM WALLOPS ISLAND, VIRGINIA (37.8°N, 75.5°W)

Vehicle Type	NASA 14.164 Nike-Apache	NASA 18.12 Nike-Tomahawk	NASA 14.298 Nike-Apache	NASA 18.30 Nike-Tomahawk
Launch Date	9-16-66	3-30-67	11-16-67	8-21-68
Launch Time(UT)	$15^h\ 54^m$	$19^h\ 09^m$	$18^h\ 14^m$	$21^h\ 30^m$
Apogee (km.)	167	239	164	268
Pulse Probe Geometry	Cylindrical	Cylindrical	Spherical	Spherical
Langmuir Probe Radius(in.)	0.25	0.25	.05	0.20
† K_p	2(Q)	2	2	1+(Q)
† A_p	10	11	9	4
† Pr.Rz	57	130	119	138

K_p = three-hour planetary geomagnetic activity index

Q = one of the ten selected geomagnetically quiet day for month

A_p = linear daily geomagnetic activity index

Pr.Rz = provisional sunspot number

† obtained from data published in the Journal of Geophysical Research (J. V. Lincoln)

techniques of the Langmuir probe, it is generally not feasible to obtain electron energy distributions in the ionosphere for energies greater than ∿1 ev. This is because of the contribution from the positive ions to the total observed current.

Hinteregger (1960) employed a gridded probe of planar geometry mounted at the nose of an Aerobee Hi rocket, which with suitably applied potentials to the grids, selectively collected particles by charge and energy. The results from this planar retarding potential analyzer indicated large departures from the thermal Maxwellian distribution for energies greater than a few ev in both the E and F regions into which the experiment was conducted.

Bowen, Boyd, Henderson and Willmore (1964) have measured the second derivative of the current to an unscreen collector electronically in an experiment conducted onboard an Ariel satellite. Their method utilized small AC potentials superimposed on a slowly varying retarding probe potential and by monitoring the pertinent AC components of the current, they were able to detect the second derivative directly. They concluded that, for altitudes somewhat greater than 350 km, any non-Maxwellian tail in the electron energy distribution involves less than one percent of the electrons,below the detection level of their instrumentation.

The pulse probe that has been developed and test flown by Bettinger (1964) consists of a central collector surrounded by two closely spaced screen girds and an outer cage. The probe as a whole is immersed in the plasma and a linear potential sweep is applied to the probe with respect to the vehicle. When operated in its DC mode,

electron energy distributions can be derived from the retarding current-voltage characteristics for the energy range of 0 - 15 ev. In the AC or pulse mode of operation, a fast negative pulse is applied to the two outermost elements of the probe and as a result, the electrons inside the effective probe volume are swept to the collector. The fast pulse technique allows the selection of electrons by their charge as well as by their relatively smaller mass. Negative ions if present inside the effective volume, for instance, will not be sensed by the collector because of their greater inertia. This pulsing action imparts energy to the heavier ionic constituents, but otherwise provides a direct electron density measurement that is independent of the electron temperature or energy distribution which is not the case for the flux type measurement conducted in the DC mode of operation. The measured concentration of electrons is that found inside the probe and to obtain the ambient electron density, we require the current corresponding to the probe at plasma potential.

The basic payload configuration was approximately the same for the four rocket experiments (Figure 1.1). The pulse probe was mounted on the top of the payload section covered by the nose cone during the flight through the lower atmosphere. At an altitude of approximately 100 km, the nose cone is ejected and the pulse probe is exposed to the plasma. The thermal equalization probes were attached to the arms on the sides of the payload section, which were recessed into the payload in their down position. They were protected by covers which were ejected upon the erection of the arms. The only significant changes among the payloads were in the placements of the

PULSE PROBE

STEP 2

C TEP 2

STEP 2

CTEP 1

$9\frac{1}{2}''$

STEP I

Langmuir Probe
Diameter = 0.5"

45°

90°
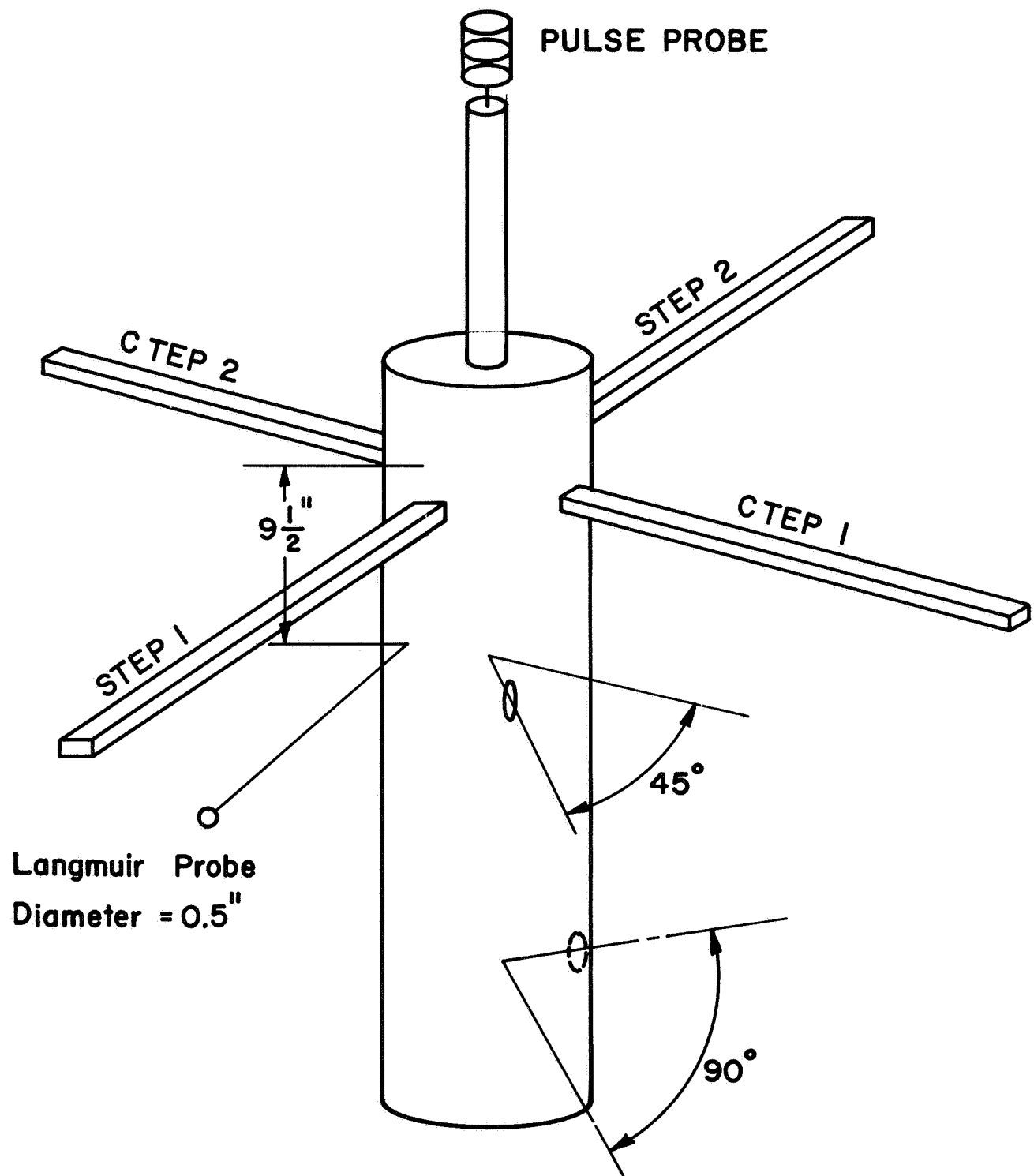
Fig. 1.1A   N/T 18.12 PAYLOAD SECTION

STEP 2

UMBILICAL

45°

CTEP 2

30°

CTEP 1

LANGMUIR
PROBE

45°

EYE

STEP 1

TOP VIEW

C TEP & STEP'S
are orthogonal

PULSE PROBE

22"

36"

TEP'S

10"

17"

13"

TO TOP OF TEP ARMS

LANGMUIR
PROBE

ASPECT EYE

All longitudinal measurements
are given using the TOP of the
TEP arms as reference plane.
TEP'S are 90° to body.

UMBILICAL

SIDE VIEW
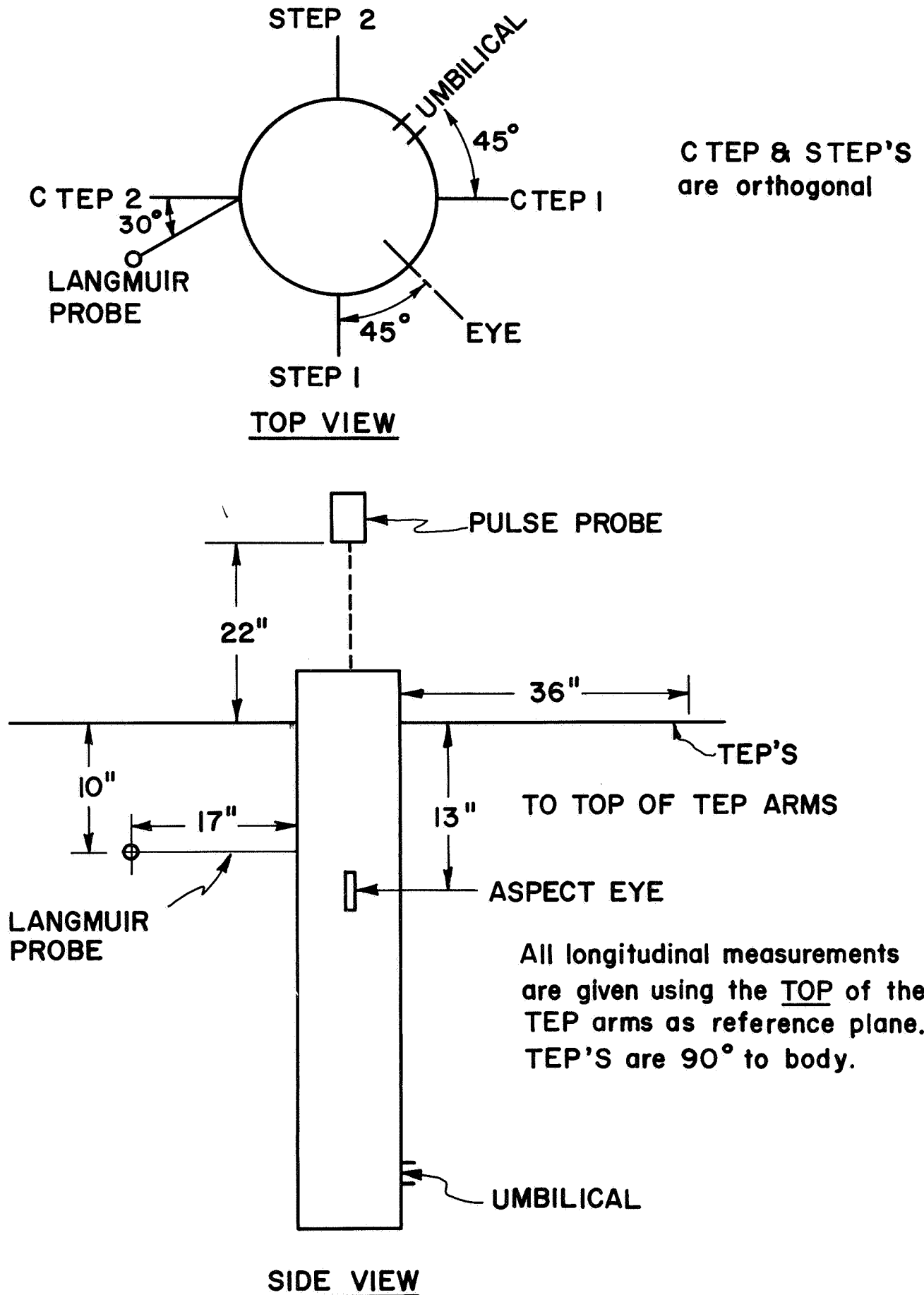
Fig. 1.1B N/T 18.12 PAYLOAD SECTION

Langmuir probes. In 14.164 and 18.30, they were situated near the pulse probe prior to probe erection (Figure 1.2). In 18.12, it was placed under the arm of a thermal equalization probe; and in 14.298, it took the place of a thermal equalization probe on one of the four mutually perpendicular arms.

For all four launches, the payload housings and the second stage rockets had conductive finishes (Figure 1.3). This was to provide a stable potential reference for the probe sweeps. A few seconds after payload despin (to 1-2 rps) the nose cone was ejected, and an onboard motor was utilized for the deployment of the arms. Figure 1.4 shows the arm fully deployed for payload 18.12 shortly after undergoing a spin test.

The four rocket vehicles performed satisfactorily in terms of their planned trajectories. Two payloads (14.164 and 14.298) had attained altitudes to the base of the F region ($\sim$ 167 and 164 km, respectively) and two (18.12 and 18.30) had penetrated into the F region ($\sim$ 239 and 268 km, respectively). They provided approximately 5 to 6 minutes of data collection time per flight. Payloads 14.164 and 14.298 had good data acquisition from all of the probes throughout their entire flights. The 18.12 and 18.30 payloads included an additional set of experiments consisting of four Langmuir probes of various sizes and geometries. They were designed and constructed by GCA. In both flights, the additional Langmuir probe experiments had premature probe erections during launch and as a result, the electronic packages suffered damages from overheating and did not acquire any useful data.
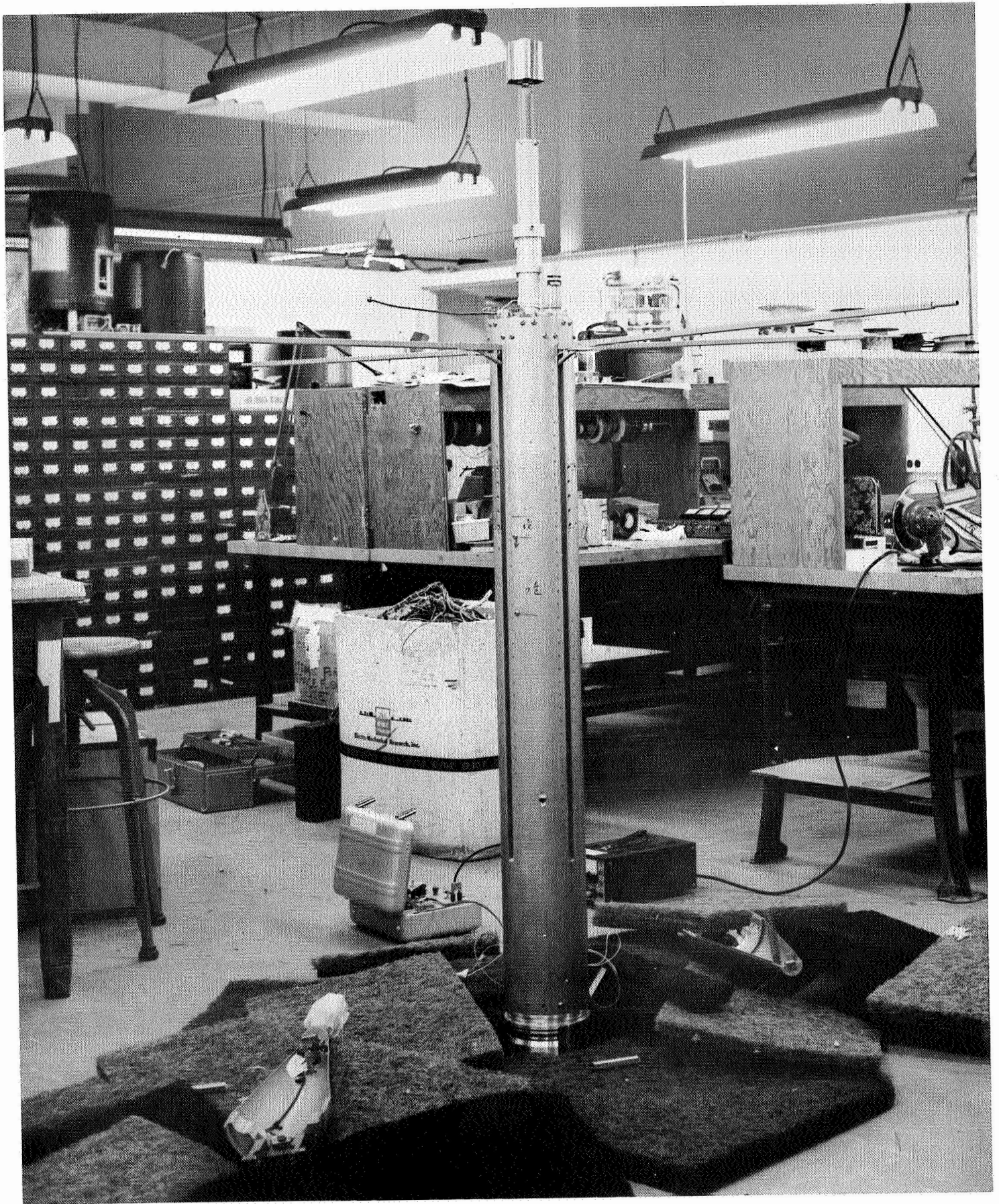
Figure 1.2 PAYLOAD SECTION (NASA 14.164)
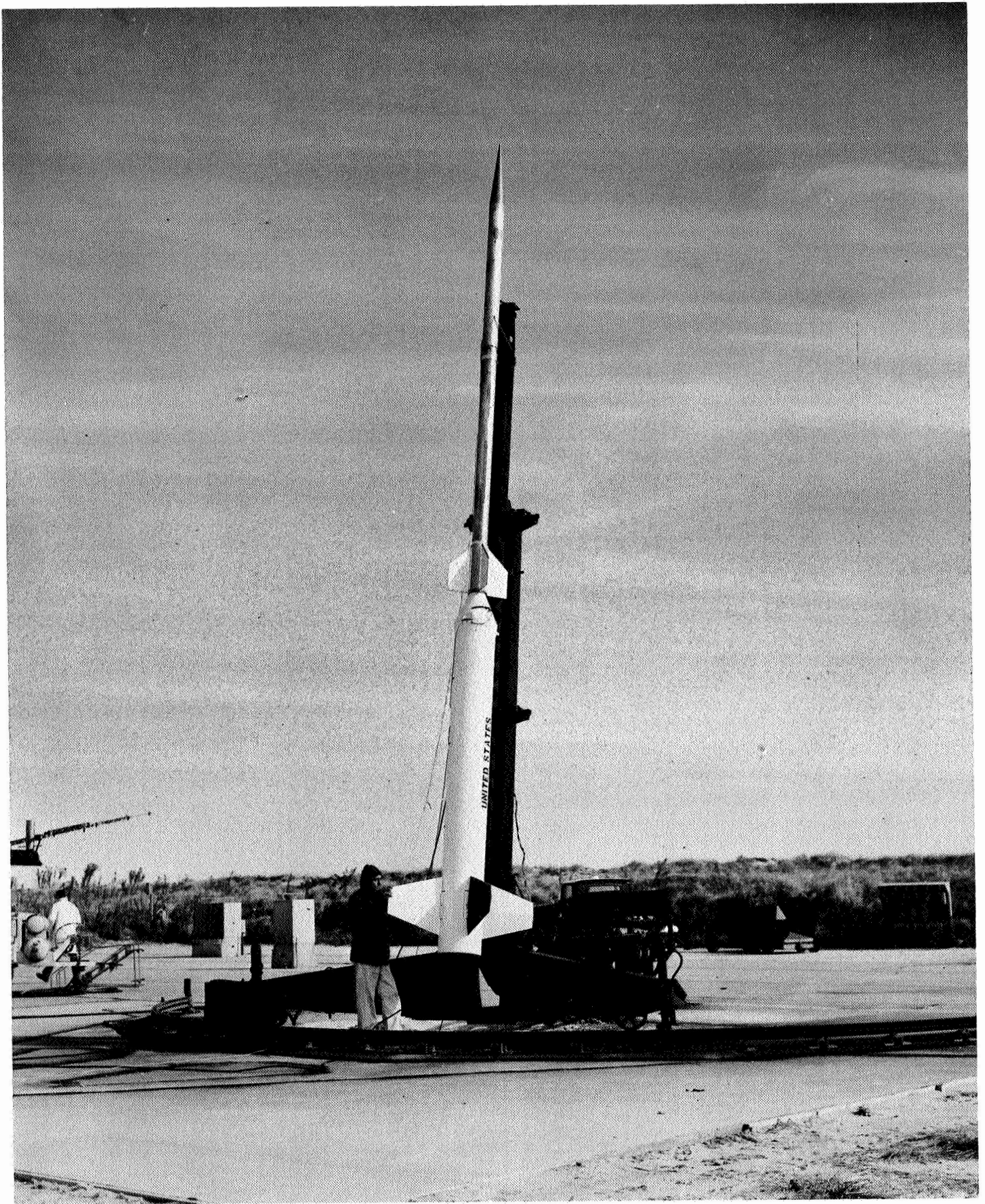
Figure 1.3   NIKE-APACHE (NASA 14.298)

Figure 1.4 PAYLOAD SECTION (NASA 18.12)

The other experiments that were conducted aboard flights 18.12
and 18.30 also encountered failures of the probe erection mechanisms,
with the result that only some of the probes had proper exposures and
adequate distances from the vehicle. The failure aboard 18.12 was
probably due to some obstruction which prevented proper arm erection
and caused the motor to become jammed. The 18.30 malfunction is
suspected to be the failure to release a restraining strap that was
designed to hold the arms in place before erection.

As a consequence, the pulse probe carried aboard 18.12 was limited
to electron energy distribution measurements. The data from the
thermal equalization probes from this flight were rendered totally
useless because of the probes' close proximity to the vehicle skin.
The Langmuir probe aboard 18.12, however, had proper erection and
performed in excellent manner for the entire flight. This particular
probe was mounted under one of the thermal equalization probe arms
and evidently the arms had moved enough to allow this probe to slip
out.

The 18.30 payload, together with probe erection failure, also
had developed noise problems in many of the subcarrier channels.
Although the pulse probe electrometer data was not greatly effected
by this noise problem, the exact usefulness of this data is questionable
because of the Langmuir probes' failure to release properly from their
locked positions. As a result of this interference caused by their
being too close together, the 18.30 payload failure was catastrophic.

CHAPTER II

THE PULSE PROBE

A. Introduction

A large variety of gridded probes have been employed for determining

the concentration and energy distribution of the plasma particules

found in the terrestrial ionosphere and in the interplanetary plasma

(Hinteregger, 1960; Sagalyn, et al., 1963; Hanson, et al., 1964;

Bettinger, 1964; Knudsen and Sharp, 1967; Harris, et al., 1967; Shea,

et al., 1968; and Moss and Hyman, 1968). This class of probes which

is commonly referred to as "retarding potential analyzers," represents

a step in sophistication from the Langmuir probes in that they attempt

to separate the components of the plasma through charge and energy

selection. This is accomplished by impressing various potentials on

the different elements of the probe and for a particular mode of

operation, the current to the collector is controlled by varying the

retarding voltage on one of the probe elements. An analysis is then

performed on the current-voltage characteristic in much the same manner

as in the treatment of Langmuir probe data, except the need to separate

the ion and electron contributions to the total collector current, for

instance, has been eliminated.

The most important advantage of utilizing the retarding potential

analyzers is that retarded current characteristics may be obtained for

positive ions (as in the ion mode of operation) and for suprathermal

electrons (if operated in the electron mode). However, by the inclusion

of one or more screens about the collector, the probe suffers from

incomplete transparency as well as such effects as secondary and

photoelectric emission from the various probe elements. These secondary effects, which may have important influence on the data and its interpretation, are extremely difficult to evaluate quantitatively. The emphasis has been to select materials with high work functions and to restrict as much as possible the probe support structures and to insure that the vehicle body is not in the probe's field of view.

The pulse probe consists of an outer cage and two closely spaced grids that surround the collector as shown in Figure 2.1. The collector was rhodium plated with a diameter of approximately 0.8 in. The two inner grids were made from stainless steel wires, and were located approximately 0.55 and 0.65 in., respectively, from the axis of the probe. The outer cage was supported by three insulated circular rings providing the probe with overall dimensions of approximately 2.9 in. in height and 2.8 in. in diameter. The cylindrical probes were flown aboard 14.164 and 18.12, while spherical probes were employed on 14.298 and 18.30. In each of these flights, the probes were programmed for two modes of operation, both for obtaining electron characteristics. The DC mode and the pulse mode of operation will be described in some detail in the following section.

B. Principles of Operation

    1. DC Mode

        In this mode of operation, the two outermost elements of the probe are kept at the same potential. The collector is biased some 26 volts positive with respect to the inner grid as shown in Figure 2.2. The probe as a whole, is swept with respect to the vehicle from approximately 3 volts positive to 13 volts negative. This linear sweep
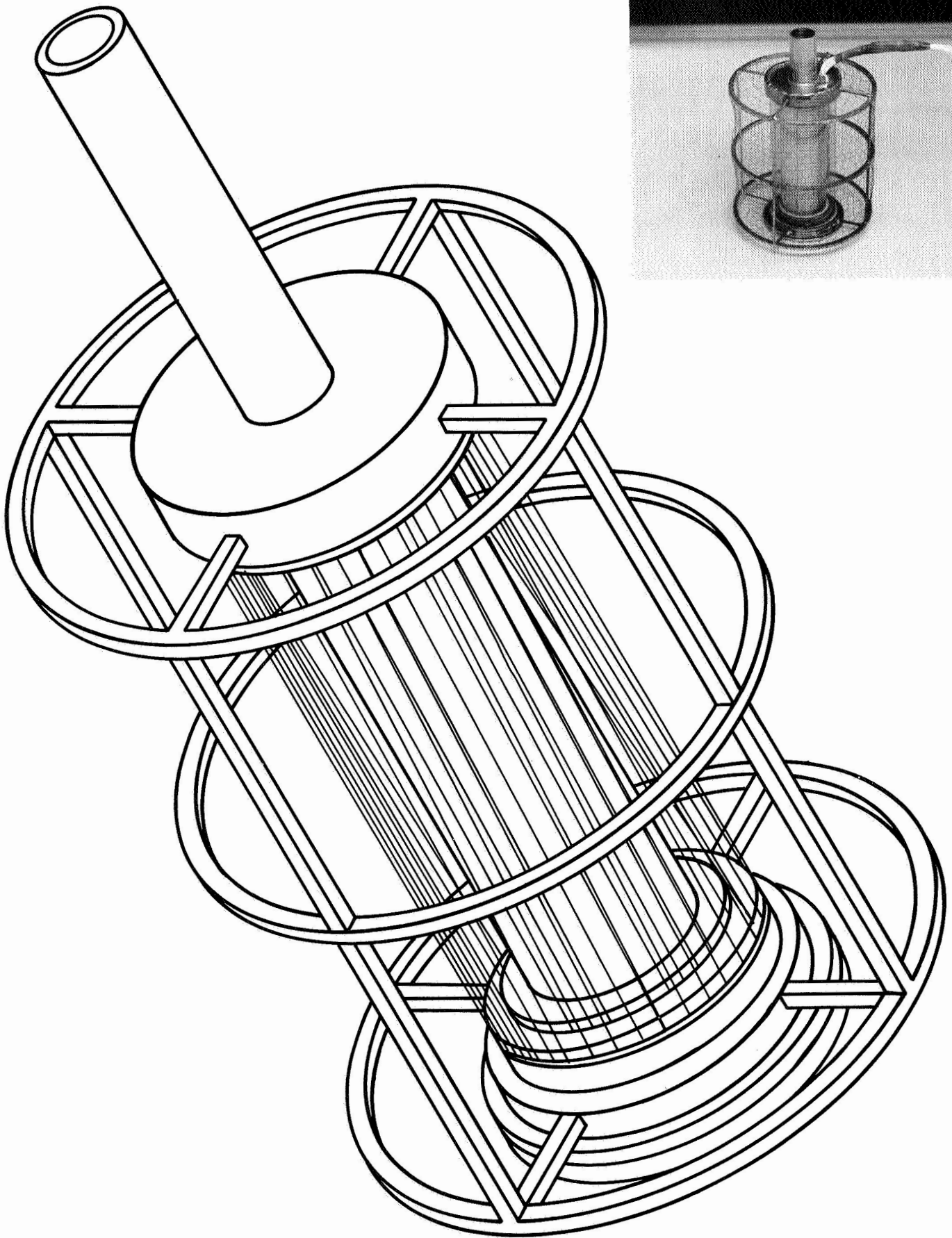
Fig. 2.1 THE PULSE PROBE
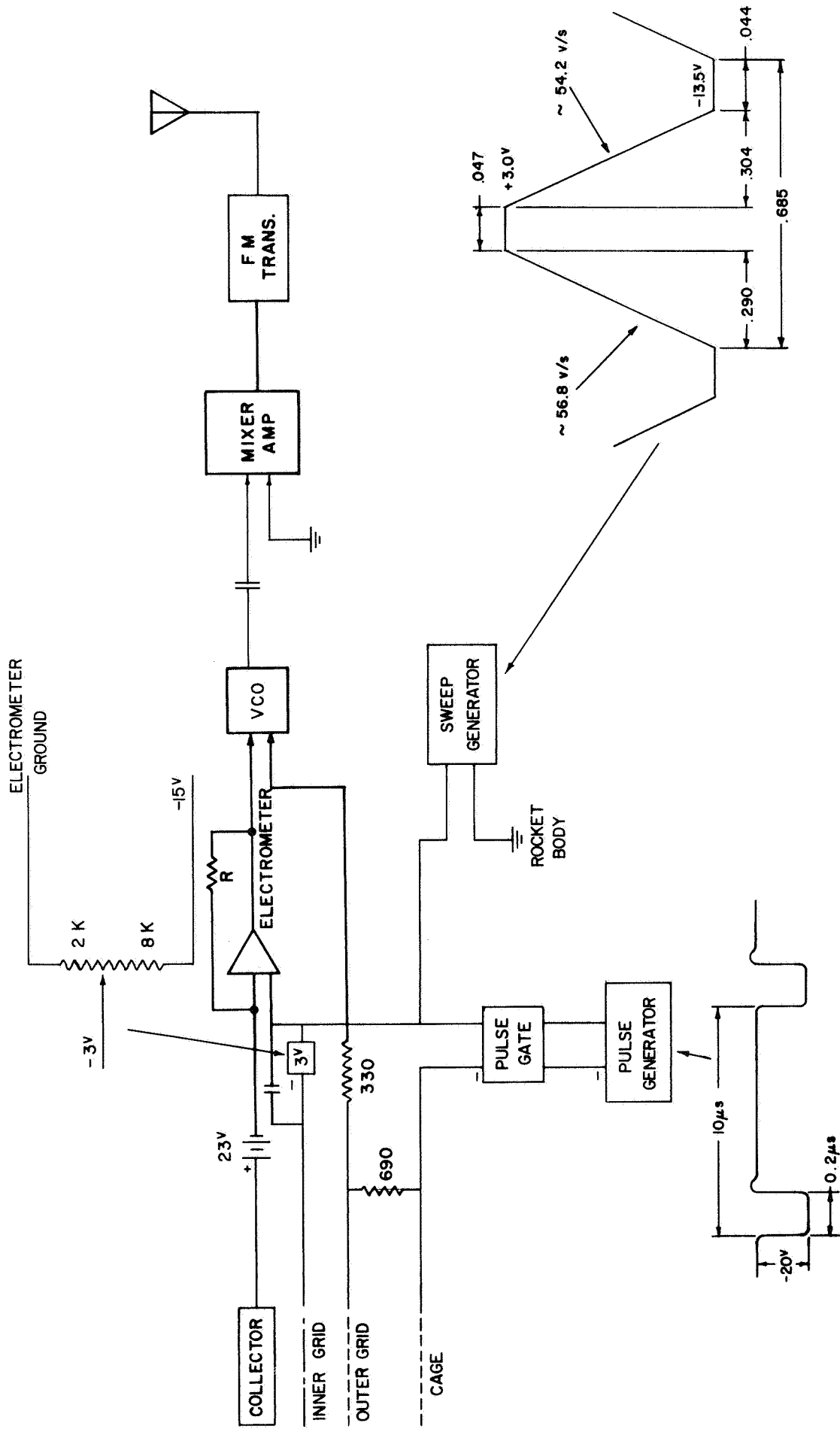
PULSE PROBE OPERATION

Fig. 2.2

has a slope $\frac{dV}{dt}$, of approximately -54 volts/sec. Under this arrangement
of potentials, positive ion penetration to the collector, as well as
photoelectric and secondary emission from the collector, are kept at a
minimum. The grid support structures were insulated and the emission
by the grids themselves are assumed to be negligible because of their
small physical area. Displacement currents associated with the sweep
were observed prior to flight and during the flight before probe
exposure and were found to be small ($< 2 \times 10^{-10}$ amps). The current
to the collector above the detection level, is primarily that due to
ambient electrons that have sufficient energy and proper direction of
incidence, to surmount the potential barrier set up by the sweep.

Figure 2.3 shows a sample of the telemetered data obtained
at an altitude of approximately 200 km from the pulse probe aboard
18.12. The collector current that is displayed at the top, was
monitored by a fixed range electrometer. The sweep voltage with
respect to the vehicle is shown at the bottom.

The sensitivity of the electrometer is periodically
switched, each range lasting approximately 0.7 seconds, synchronized
with the period of the voltage sweep on the probe. The probe is
operated in the pulse mode during the first half of this period and
in the DC mode during the latter half. The electrometer's sensitivity
is controlled by the value of the feedback resistor R, located between
the input and the output terminals of the operational amplifier. The
values chosen for the feedback resistors were 10^5, 10^6, 10^7, 10^8, and
10^9 Ω, given here in the order of the switching sequence. The value
at the output of the operational amplifier corresponding to electrometer

PULSE
PROBE
CURRENT

ELECTROMETER
SATURATION

ZERO CURRENT
CALIBRATIONS

PULSE PROBE
SWEEP

10^{-5} R

10^{-6} R

10^{-7} R

10^{-8} R

10^{-9} R

PULSE
MODE

DC
MODE

TIME (SECONDS)
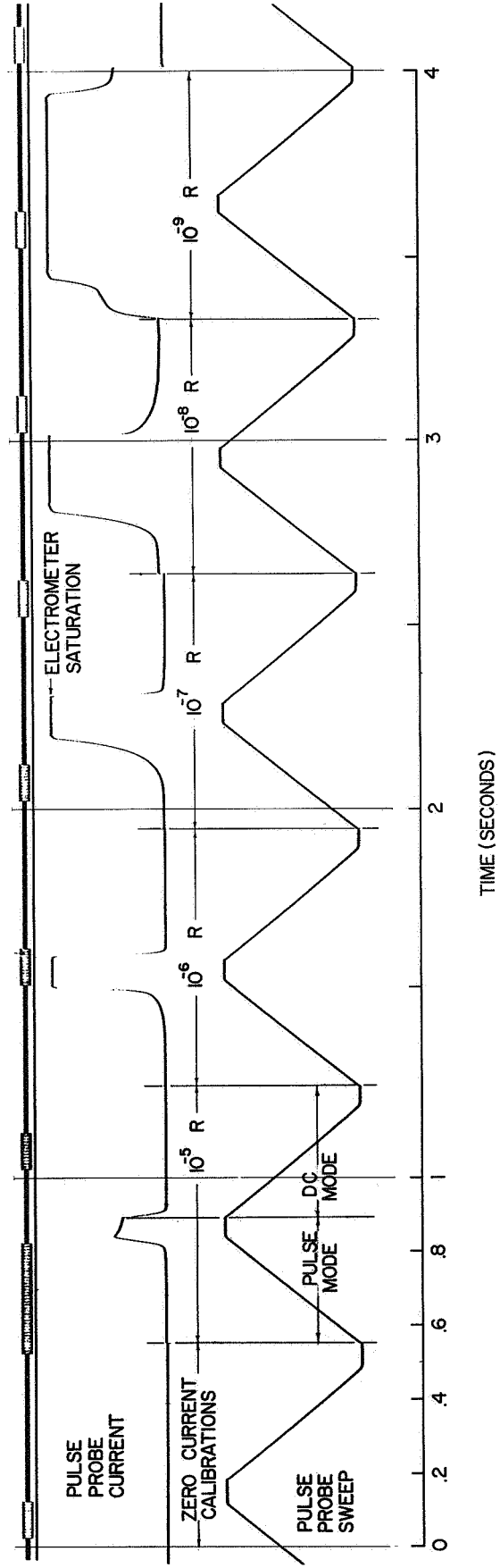
Fig. 2.3   SECTIONS OF RAW PULSE PROBE DATA

AT ALTITUDE ~ 200 KM

saturation was approximately 5.7 volts. Thus, the sensitive range of

the electrometer for a particular feedback resistance of value R

($\sim 10^5$, 10^6, 10^7, 10^8, 10^9 Ω), is from zero to (5.7/R) amps and with

each successive switching of the value of R, we effectively increase

the sensitivity or full scale by a factor of approximately ten. Zero

current calibrations were taken at the beginning and at the end of

each series of range switching.

2. Pulse Mode

In the pulse mode of operation, which is in effect during the

first half of each electrometer range where the potential sweep is

increasing in time, a negative square wave of approximately 20 volts

in amplitude is applied to the outer cage relative to the inner grid.

This 20 volts is divided between the three outer probe elements such

that the potential difference between the outer cage and the outer

grid is approximately 13 volts and that across the outer grid and the

inner grid is about 7 volts. The pulse frequency is 100 kc per second,

with a pulse duration of approximately 0.2 μ seconds. Thus, for the

duration of the pulse, all electrons inside the probe are accelerated

toward the collector and those outside the cage, near the probe, are

repelled away from the vicinity of the probe. In order to suppress

current collection in between pulses, a negative potential of

approximately 3 volts is applied to the inner grid relative to the

outer grid. The effect of the pulse on ion motion, for the most part,

can be considered negligible because of their relatively large inertia.

The density of the electrons n_p, inside the cage can be expressed

as a linear function of the pulse current I_p, by

$$n_p = \frac{I_p}{\alpha e f V_{eff}} \tag{2.1}$$

where V_{eff} is the effective probe volume, f is the pulse repetition

rate, e is the electronic charge and α is the combined transparency

of the two inner grids that surround the collector. The density n_p

inside the effective volume of the probe is equal to the density

immediately outside the cage surface multiplied by the transmission

coefficient of the cage. Here we have assumed that the collection

voltage and the pulse duration are sufficiently large to permit the

collection of all the electrons inside the effective probe volume,

and that collisions within the probe are negligible. Strictly speaking,

because of angular momentum and energy conservation, it is not

possible to collect all the electrons within the probe, i.e., those

with high energy and very large angular momentum. However, for the

thermal electrons (T ∿ 2000°K), for which the applied collection

potential is much greater than their average energy, a pulse duration

of 0.2 μ seconds provides sufficient time for most of these electrons,

if not all, to reach the collector before the termination of the

pulse. For instance, the time it takes for an electron initially at

rest located near the outer cage to travel to the collector can be

shown to be approximately 5×10^{-9} seconds from the application of

20 volts across the outer probe elements (Bettinger, 1964).

The total collector current in the pulse mode may be written

as:

$$I_t = I_p + (\Delta t) fI_o + [1 - (\Delta t)f]I_b , \qquad (2.2)$$

where the first term I_p is the pulse current given by equation (2.1).

The second term on the right-hand side represents the current due to

those electrons that entered the probe while the pulse was applied and

the third term is the collection of electrons during the time period

between the application of the pulses. The term $(\Delta t)f$ is the fraction

of the time when the pulses were employed, where Δt is the pulse

duration, and f is the pulse repetition rate. The second term may,

for all practical purposes, be neglected since I_o represents the

collection of electrons with energies greater than the pulse potential

plus the sweep potential and $(\Delta t)f \sim 0.02$. Thus, the pulse current I_p

may be obtained simply by subtracting from the measured total collector

current the third term in equation (2.2), where I_b is the current

detected in the DC mode of operation.

The special advantage of the pulse technique is that the density

measurement is made independent of the velocity distribution of the

particles. Furthermore, the pulse current I_p, as a function of the

sweep potential, shows a maximum at the plasma potential and should be

readily identifiable so that the ambient density may be obtained without

independent knowledge of the vehicle to plasma potential.

C. Probe Theory

In this section we will review the general theory of probe currents

beginning with a brief discussion of the conventional Langmuir probes,

which have been employed rather extensively aboard sounding rockets

and satellites for the measurements of electron temperature and

concentration (Spencer, et al., 1962; Spencer, et al., 1965; Bettinger, 1965;

Smith, 1966; Bettinger and Chen, 1966; Smith, et al., 1967). This will be

followed by a derivation of the Druyvesteyn relationship, which may be

used for obtaining the energy distribution of the plasma particles

from the retarding current-voltage characteristic such as that obtained

with the pulse probe. We shall be primarily concerned with the case

where the probe can be considered stationary and where the mean free path of the plasma particles is sufficiently large that collisions within the charged sheath associated with the probe may be ignored.

1. Langmuir Probe

The Langmuir probe is an unscreened collector that is inserted into the plasma and the current as a function of the applied voltage is recorded for analysis. When it is carried aboard a sounding rocket or satellite, the applied potential is usually referenced to the vehicle skin and the current is then obtained as a function of the probe to vehicle potential. The collector is frequently accompanied by a guard electrode that is maintained at the same potential as the collector to minimize any interaction with the probe support structure.

Mott-Smith and Langmuir (1926) have treated the basic theory of collectors with simple goemetries immersed in ionized gases. They have derived various expressions for the probe current as a function of probe to plasma potential corresponding to different velocity distributions for the plasma particles. In the following, we shall restrict our attention to the case where the plasma particles are mainly electrons and singly charged positive ions having Maxwellian velocity distributions.

Since the average speed of the electrons is, in general, greater than that of the positive ions, a body or probe immersed in the plasma will acquire a negative equilibrium potential. The presence of this negative charge on the probe is shielded from the rest of the plasma by a positive space charge region surrounding the probe. When

the probe potential is varied relative to the plasma, the sheath thickness will change accordingly, and in particular, when the probe is made positive, the net charge of the sheath will then be negative. The total probe current at any given probe potential is the sum of the electron current and the ion current. For the charge particles within the sheath region, one component will be accelerating, while for the other, retarding.

The accelerating current to a spherical probe of radius r, for a Maxwellian distribution of n particles per unit volume, and temperature T, as given by Mott-Smith and Langmuir (1926) may be written as:

$$i = 4\pi a^2 I_o \left[1 - \left(\frac{a^2 - r^2}{a^2} \right) \exp\left(- \frac{r^2 \psi}{a^2 - r^2} \right) \right] , \quad (2.3)$$

where $I_o = \frac{n e \bar{v}}{4} = ne \left(\frac{kT}{2\pi m} \right)^{1/2}$ the thermal current per unit area, a is the sheath radius, $\psi = \frac{eV}{kT} > o$, V is the probe to plasma potential, k is the Boltzmann constant, with e and m being the particle's charge and mass, respectively. We see that the first term in equation (2.3) is simply the current incident to the sheath surface and the current to the probe is this quantity reduced by the exponential term. The sheath radius a is, of course, a function of the probe to plasma potential V, as well as the parameters characterizing the plasma such as density and temperature. Expressions for the sheath thickness have been derived by Bettinger and Walker (1965) and can be utilized here for calculating the current i as a function of the probe potential V.

For a Maxwellian distribution, the current due to the particles

under retardation can be expressed as:

$$i = 4\pi r^2 I_o e^{\frac{-eV}{kT}} , \qquad\qquad (2.4)$$

where V is the value of the retarding probe potential, and I_o is the thermal current given above. A plot of log i as a function of the potential V will result in a straight line whose slope is inversely proportional to the temperature T.

Electron temperatures are usually obtained from the Langmuir probe characteristics with the use of equation (2.4). In the ionospheric plasma, the probe current due to electrons dominate at or near plasma potential, and the retarded electron current is normally extracted from the total current by subtracting from it the smaller ion contribution. This is often accomplished by extrapolation of the experimental curve of the total probe current from some large negative value of probe potential, where the electron contribution can be assumed to be negligible, and taking the extrapolated curve as the ion current. Having obtained the retarded electron current near plasma potential, the slope is then calculated, and from it, the electron temperature.

The density n can be estimated from the thermal current expression for I_o, if T is known, as well as where the point of plasma potential is located on the characteristic. However, due to surface imperfections of most probes, this is often a very difficult task (F. Huang, 1969).

    2. Druyvesteyn Relationship

For a probe with a negative potential V, relative to the

plasma, ambient electrons with energies $E \geq eV$, and the proper directions

of incidence may reach the probe surface and contribute to the probe

current. Druyvesteyn (1930) showed that the electron velocity

distribution of an isotropic plasma can be found by taking the second

derivative of this current with respect to the retarding probe potential.

The results are equally applicable for obtaining the ion distribution

from the retarded ion current and for the case of a spherical probe

immersed in an anisotropic distribution. Here we shall consider only

the derivation for the cylindrical probe in an isotropic velocity

distribution, neglecting any end effects. Identical relations may be

shown for other standard probe geometries.

Let $f(v)d^3v$ be the number of electrons per unit volume in the

ambient plasma with velocities between $\vec{v}$ and $\vec{v} + d\vec{v}$ such that the

normalization condition can be expressed as:

$$\int_{\text{all vel.}} f(v)d^3v = n \, , \tag{2.5}$$

where n is the ambient electron concentration. Taking the usual

cylindrical coordinate system, and letting v_ρ be positive, when it is

directed into the collector, the electron current to the collector may

be written as:

$$i = 2\pi a\ell e \int \int \int_\alpha v_\rho \, g(v_\rho, v_\phi, v_z) \, dv_\rho \, dv_\phi \, dv_z \, , \tag{2.6}$$

where g is the ambient velocity distribution function expressed in terms of the cylindrical velocity components, ℓ is the length of the collector, a is an arbitrarily chosen radius located anywhere outside the cylindrical sheath surrounding the probe where the distribution is undisturbed, e is the electronic charge, and α specifies the fraction of the current incident on the arbitrary surface that actually reaches the collector consistent with conservation of angular momentum and energy. If α was chosen to include all velocities directed inward, then i would express the current to the surface defined by the radius a and the length ℓ.

From conservation of angular momentum, we have

$$v_\phi(a)a = v_\phi(R)R \ , \tag{2.7}$$

where R is the radius of the probe, and by conservation of energy, we obtain the following equation:

$$\tfrac{1}{2}mv^2(a) = \tfrac{1}{2}mv^2(R) + eV \ , \tag{2.8}$$

where m is the electronic mass, and V denotes the retarding probe potential. Since the field is radial,

$$v_z(a) = v_z(R) \ , \tag{2.9}$$

and we may rewrite equation (2.8) as:

$$v_\rho^2(a) + v_\phi^2(a) = v_\rho^2(R) + v_\phi^2(R) + \frac{2eV}{m} \ .$$

Substituting for $v_\phi(R)$ from equation (2.7), this becomes

$$v_\rho^2(R) = v_\rho^2(a) + v_\phi^2(a) \left(1 - \frac{a^2}{R^2} \right) - \frac{2eV}{m} \quad . \tag{2.10}$$

For a particle to be collected, we require that $v_\rho(R) \geq o$ or, from equation (2.10) that

$$v_\rho(a) \geq \sqrt{v_\phi^2(a) \left(\frac{a^2}{R^2} - 1 \right) + \frac{2eV}{m}}$$

for a given value of $v_\phi(a)$. Therefore, in the case of a cylindrical collector, where the end effects can be ignored, the current

$$i = 2\pi a\ell e \int_{-\infty}^{+\infty} \int_{-\infty}^{+\infty} dv_\phi dv_z \int_\alpha^{+\infty} v_\rho\, g(v_\rho, v_\phi, v_z) dv_\rho \quad ,$$

where $\alpha = \sqrt{v_\phi^2 \left(\frac{a^2}{R^2} - 1 \right) + \frac{2eV}{m}}$. Making use of the Leibnitz Rule

$$\frac{d}{dt} \int_{x_1(t)}^{x_2(t)} k(x)dx = k(x_2)\frac{dx_2}{dt} - k(x_1)\frac{dx_1}{dt} \quad , \tag{2.11}$$

we get $\frac{di}{dV} = - \frac{2\pi a\ell e^2}{m} \int_{-\infty}^{+\infty} \int_{-\infty}^{+\infty} dv_\phi dv_z\, g(\alpha, v_\phi, v_z)$ \hfill (2.12)

since $\frac{d\alpha}{dV} = \frac{e}{m\alpha}$.

If the velocity distribution function is isotropic, then

$$g(\alpha, v_\phi, v_z) = f(v), \text{ where } v^2 = \alpha^2 + v_\phi^2 + v_z^2 = \frac{a^2}{R^2} v_\phi^2 + v_z^2 + \frac{2eV}{m} .$$

Let us define $\gamma = \frac{a}{R} v_\phi$, with $d\gamma = \frac{a}{R} dv_\phi$. Then we may write equation

(2.12) as:

$$\frac{di}{dV} = - \frac{2\pi R\ell\, e^2}{m} \int_{-\infty}^{+\infty} \int_{-\infty}^{+\infty} d\gamma\, dv_z\, f(v). \qquad (2.13)$$

This may be readily reduced to an expression involving a single integral, with $A = 2\pi R\ell$,

$$\frac{di}{dV} = - \frac{2\pi A e^2}{m} \int_{\sqrt{\frac{2eV}{m}}}^{+\infty} dv\, v\, f(v) \quad . \qquad (2.14)$$

Differentiating again and applying the relationship given by equation (2.11), we obtain

$$\frac{d^2 i}{dV^2} = \frac{2\pi A e^3}{m^2}\, f\left(\sqrt{\frac{2eV}{m}}\right) \quad . \qquad (2.15)$$

Thus, if we plot $\left\{\frac{d^2 i}{dV^2}\right\}$ as a function of $\left\{\sqrt{\frac{2eV}{m}}\right\}$, we then have the

isotropic velocity distribution function f as a function of v, except for a multiplicative constant.

Equations (2.14) and (2.15) may be transformed into terms

involving the energy distribution function F(E) by making use of the

following relations: $E = \frac{1}{2}mv^2$, or $dE = mvdv$, and

$$4\pi f(v) \, v^2 dv = F(E)dE, \text{ or } f(v) = \frac{m^{3/2} \, F(E)}{4\pi (2E)^{\frac{1}{2}}} \quad . \text{ Thus, for equation (2.14)}$$

we have
$$\frac{di}{dV} = - \frac{Ae^2}{2(2m)^{\frac{1}{2}}} \int_{eV}^{+\infty} \frac{F(E)dE}{E^{\frac{1}{2}}} \quad , \tag{2.16}$$

and equation (2.15) becomes
$$\frac{d^2i}{dV^2} = \frac{Ae^3 F(eV)}{2(2meV)^{\frac{1}{2}}} \tag{2.17}$$

or,
$$F(E) = \frac{2(2mE)^{\frac{1}{2}}}{eA} \frac{d^2i(V = E/e)}{dE^2} \quad , \tag{2.18}$$

where F(E) satisfies the normalization condition:

$$\int_o^\infty F(E)dE = n \quad . \tag{2.19}$$

For an arbitrary energy distribution function F(E), we see

from equation (2.16) that the slope will always be negative and therefore,

the current will always monotonically decrease with increasing retarding

probe potential. Furthermore, the magnitude of the slope must also

decrease momotonically as the retarding probe potential is increased.

If for a particular distribution function F(E), such that it

vanishes in the energy interval between E_1 and E_2, then in the range of

retarding probe potentials between $V_1 = \dfrac{E_1}{e}$ and $V_2 = \dfrac{E_2}{e}$, the slope

$\dfrac{di}{dV}$ is a constant, or the current is a linear function of the

retarding probe potential.

From equation (2.18) it is readily seen that if the current

was an exponential function of the retarding probe potential, then the

resulting energy distribution is Maxwellian. It is also apparent that

the distribution function obtained by taking the second derivative of

the probe current is uneffected by the addition of either a constant

or linear term to the total probe current.

CHAPTER III

PULSE PROBE DATA

A. Introduction

In the first part of this chapter, we will discuss the acquisition
and the processing of the experimental data as obtained by the pulse
probe. The vast amount of data that has been acquired, even from a
single flight payload, has necessitated the use of some kind of
automatic processing equipment. We have available within the Atmospheric
Physics Group a CDC-160 computer which is directly linked to an analog
to digital conversion system. Utilizing this system, the raw analog
data was digitized and recorded onto magnetic binary tapes. Further
processing and analysis of this binary data was performed by the
CDC-160 as well as an IBM-7094 computer (Computer Science Center,
University of Maryland).

The latter part of this chapter pertains to the methods of data
analysis and some of the results of that analysis will be presented.
In particular, the electron energy distributions in the energy range
of 0-15 ev as detected with the pulse probe operated in the DC mode
will be emphasized.

We shall be concentrating most of our attention on the data
gathered from the 18.12 flight (19^h09^mUT, March 30, 1967), which had
exceptionally low noise levels in all the data channels as compared
to the results obtained from the other flights. However, on this
particular flight, the experiments with the exception of the Langmuir
probe, had insufficient probe deployment due to the failure of the

erection mechanism. As a result, the data from the thermal equalization probes were rendered totally useless because of their close proximity to the vehicle skin. Thus, it meant that we could not continuously monitor the vehicle potential and would have to assume that the vehicle to plasma potential was constant at least during the time period of one probe sweep. However, this assumption can be considered not altogether unreasonable since the area ratio of the probe to vehicle was less than 1:1000.

Although the erection failure did not have any great effect on the detection of the suprathermal electron energy distribution, it did leave the pulse probe in a position to be affected by the charged sheath associated with the vehicle. Thus, the thermal electron current to the probe is partially suppressed, eliminating any direct measurements of the ambient electron concentration.

B. Experimental Data

1. Data Acquisition

The raw data that is acquired from the experiments conducted aboard the sounding rockets were transmitted to the ground stations through the utilization of FM-FM telemetry systems. The collector current from the pulse probe, for instance, produces an output response from the electrometer amplifier in the form of a voltage signal. This output voltage modulates a voltage controlled oscillator whose output frequency varies about a preselected value (the subcarrier frequency). The signal then proceeds through a band pass filter before it is combined with those signals generated from the other subcarriers by a mixer network. This combined signal is then transmitted by a frequency modulated transmitter and received by the ground stations.

The FM signals from the outputs of the ground receivers were then recorded onto magnetic tapes. The data playbacks from these magnetic tapes can be achieved by first demodulating the composite video signals with subcarrier frequency discriminators whose voltage outputs may then be displayed on oscillographs or fed directly into an analog to digital converter whose binary information can be made acceptable to a computer such as the CDC-160 by a suitable buffer unit.

Table 3.1 lists the subcarrier assignments made for the various experiments conducted aboard payload 18.12 (standard IRIG specifications for narrow bands) and their corresponding maximum intelligence frequencies. The subcarrier 52.5 kc $\pm$ 7.5% was designated for the transmission of the pulse probe electrometer data. The frequency response of this particular subcarrier channel is approximately 790 cps.

2. Digitized Current-Voltage Characteristics

The analog to digital conversion was performed by an Epsco Datrac (model 611) unit which has the capability for carrying out high speed conversion (with a conversion dead-time $\sim$ 25μ seconds). The digitization system consisting of the analog to digital converter, together with the buffer unit and the CDC-160 computer, was operated in the "converter limited" mode. In this mode, the rate of digitization was set by an externally generated timing pulse which was used in triggering the converter. At the termination of each conversion to a twelve bit word, the CDC-160 was programmed to directly store the digitized data into computer memory ($\sim$ 4000 available locations). Since the computer has an internal storage cycle time of approximately 13μ seconds, it will then wait until the end of the next conversion.

Table 3.1 NASA NIKE-TOMAHAWK 18.12 UI, TM FORMAT

Channel Description	IRIG Channel	Subcarrier Freq. (KC)	Low Pass Filter (CPS)
GCA Langmuir Probe	21	165	2500
GCA Langmuir Probe	20	124	1900
CTEP #1	19	93	1400
CTEP #3	18	70	1050
Pulse Probe Current	17	52.5	790
Langmuir Probe Current	16	40	600
Pulse Probe Sweep	15	30	450
Langmuir Probe Sweep	14	22	330
STEP #2	13	14.5	220
STEP #4	12	10.5	160
Housekeeping Commutator	11	7.35	110
Long. Magnetometer	10	5.4	81
Lat. Magnetometer #1	9	3.9	59
GCA Commutator	8	3.0	45
Lat. Magnetometer #2	7	2.3	35
Aspect Eye	6	1.7	25

For a conversion rate of 1 kc per second of real time data playback, it would permit the computer from one sampling of 4000 words (lasting ∿ 4 seconds) to store into memory a complete current-voltage characteristic. That is to say, the block of data stored in memory would consist of a full set of different electrometer sensitivities for the collector current together with the zero current calibration.

The computer then recorded from its memory the binary data onto magnetic tapes for further processing and analysis. The rate of conversion (1 kc per second) was more than adequate for the examination of the retarded suprathermal electron current, but only minimal with regard to the retarded thermal electron current (∿ 7 - 12 data points). If we increased the conversion rate (i.e., higher resolution), then the length of the sample record would have to be necessarily shorter because of the limited number of locations in the memory of the CDC-160 computer.

A buffered binary tape unit for the recording of the binary information, which completely bypasses the CDC-160 computer, has been built to take advantage of the high speed conversion that is possible with the Epsco Datrac Unit. With this unit in operation, it is possible to increase the rate of conversion to approximately 15 kc per second recording a continuous record on the binary tape unit and thus, greatly increasing the resolution and facilitating the data processing. For instance, it would have permitted a recording of ∿ 100 data points for the retarded thermal electron current section, but it was unavailable at the time when the data was being processed.

Figure 3.1 shows three different digitized current curves

Fig. 3.1

PULSE PROBE CURRENT vs. SWEEP POTENTIAL

NIKE – TOMAHAWK   18.12
MARCH   30, 1967

DC   MODE , ASCENT

△ 10^{-6} R

□ 10^{-7} R

• 10^{-8} R

239 Km

174 Km

126 Km

10^{-5}

10^{-6}

10^{-7}

10^{-8}

10^{-9}

PROBE CURRENT   (AMPERES)

-5.0   -4.0   -3.0   -2.0   -1.0   0   1.0   2.0

SWEEP POTENTIAL   (VOLTS)
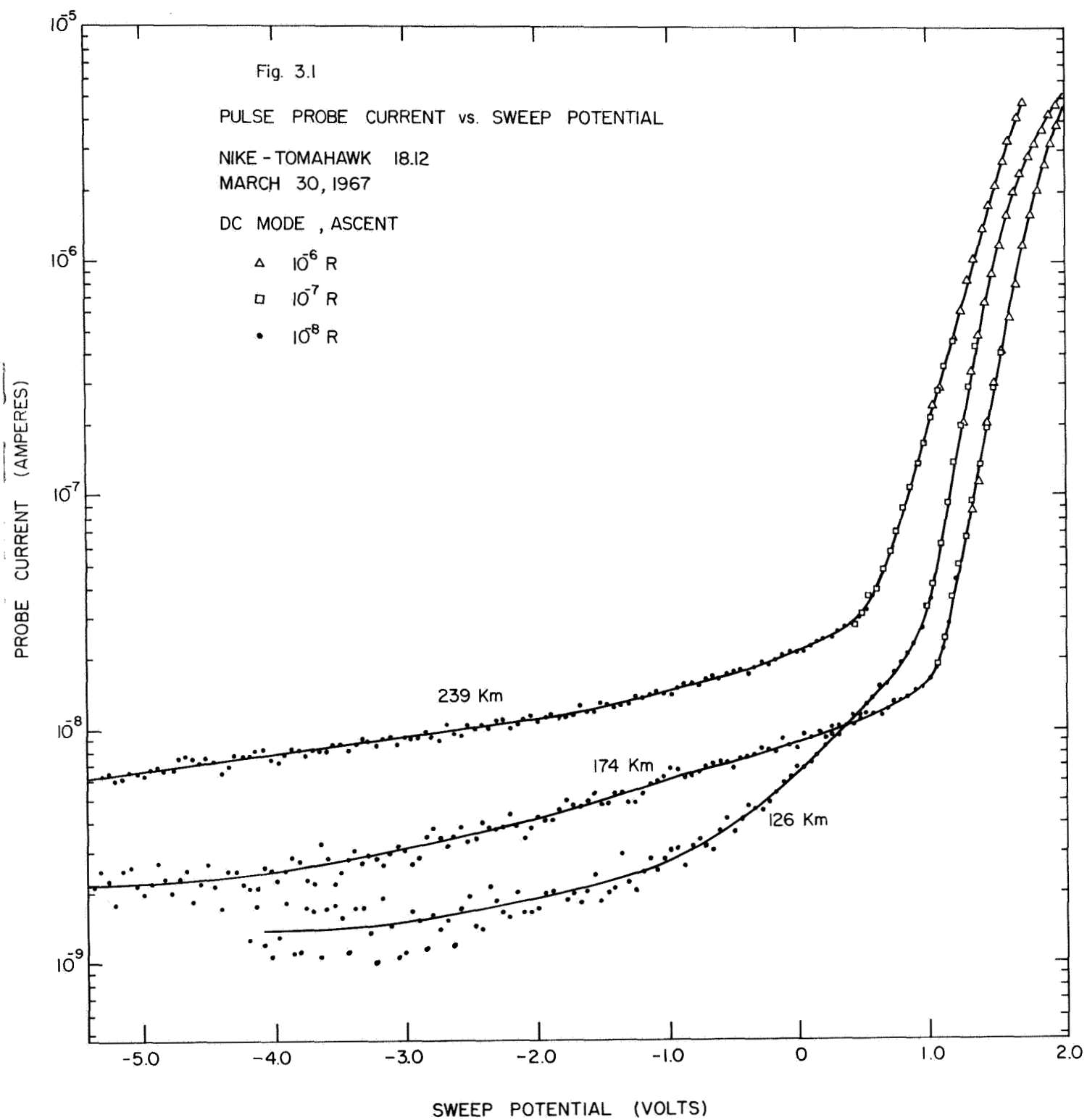
plotted logarithmically as a function of the applied sweep potential

with respect to the vehicle obtained at three different altitudes

during rocket ascent. These curves were obtained for the case where

the probe was operated in the DC mode. Each of the current curve

shown in Figure 3.1 is made up of three different sections, each

section corresponds to a different electrometer sensitivity.

Calibrations of the sensitivities and the linearity of the

electrometer were performed prior to launch. This was done by

feeding a known current into the electrometer and recording the response.

A zero current calibration level (by opening the electrometer input)

was programmed to occur before and after the sequence of range switching.

For each range of the electrometer, there exists a current level which

corresponds to electrometer saturation. Any collector current that

exceeds this level produces a fixed constant output from the electrometer.

These two reference levels, the saturation point and the zero current

level, permit the determination of the electrometer sensitivity from

which the absolute current may then be calculated.

A total of forty current-voltage characteristics, such as

those shown in Figure 3.1, were obtained and analyzed from the flight

18.12. They shall now be discussed in detail in the following section.

C. Data Analysis

In the analysis of the pulse probe data, we have assumed that the

vehicle to plasma potential was constant during the potential sweep

over the retarding portion of the curve. For flight 18.12, this has

been concluded to be reasonably valid because of the relatively large

conductive area of the reference vehicle in contact with the plasma.

An increase in the negative current collected by the pulse probe, as it
is swept toward a more positive potential, must be accompanied by an
equal amount of positive current collection by the vehicle. Thus, any
significant modulation of the vehicle potential due to the pulse probe
sweep would take place only in that section of the curve where a large
variation of the collector current occurs, such as when the probe begins
its sensing of the thermal electrons. When the vehicle has a relatively
large conductive area exposed to the plasma, only a small negative change
in its potential will be necessary to collect the required amount of
positive current provided, of course, that its equilbrium potential is not
so large that it is in the positive ion saturation region (Bettinger,1965).

We have also assumed in this analysis that the electrometer
sensitivity remained constant and equal to the value determined in the
preflight calibrations. If the variation of this quantity is small
and over long time periods, it will not seriously affect the analysis
that is performed over a given current curve, such as in the determination
of electron temperature. Significant variations would, however, affect
any density measurements which depend on the detection of absolute currents.

In Chapter II we derived the Druyvesteyn relationship which showed
that the velocity or energy distribution of the plasma particles in an
isotropic plasma can be related to the second derivative of the current
with respect to the retarding probe potential. This relationship is
also valid in the case of an anisotropic distribution, if a spherical
probe was utilized. The pulse probe that was launched aboard 18.12 had
a length to diameter ratio for the outer cage of approximately
one and a ratio for the inner collector of approximately

three. Thus, the probe closely approximates spherical geometry and any anisotropy in the distribution will not be clearly evident in the current as a function of probe aspect, and the Druyvesteyn relationship is applicable for either an isotropic or anisotropic velocity distribution. The spherical probes launched aboard 14.298 and 18.30 were undoubtably more ideal, however, from the reasons given previously their results were unsatisfactory. The probe design for 18.12 was dictated at the time more so by the ease in construction and mechanical reliability.

1. The Residual Current

For the pulse probe in the DC mode of operation, with an applied retarding potential V, relative to the plasma potential, only those ambient electrons with energies $E \geq eV$, and the proper directions of incidence will reach the surface of the inner grid and contribute to the collector current. The maximum applied retarding sweep potential was approximately 13.5 volts with respect to the vehicle and if we assume that the vehicle to plasma potential was of the order of 2 volts, this means that no information can be obtained for the energy distribution of the electrons for the energies beyond approximately 15.5 ev. As we shall see later, the pulse probe results indicated that the vehicle potential was actually slightly greater than 2 volts for most of the 18.12 flight which is in general agreement with the results obtained with the Langmuir probe.

The collector current corresponding to the maximum applied retarding potential is shown in Figure 3.2 as a function of altitude. This current is that due to ambient electrons with energies greater

Fig. 3.2

MINIMUM PROBE CURRENT
vs. ALTITUDE

NIKE - TOMAHAWK 18.12
MARCH 30, 1967

DC MODE
○ ASCENT
□ DESCENT

ALTITUDE   Km

I $(10^{-9}$ AMP$)$
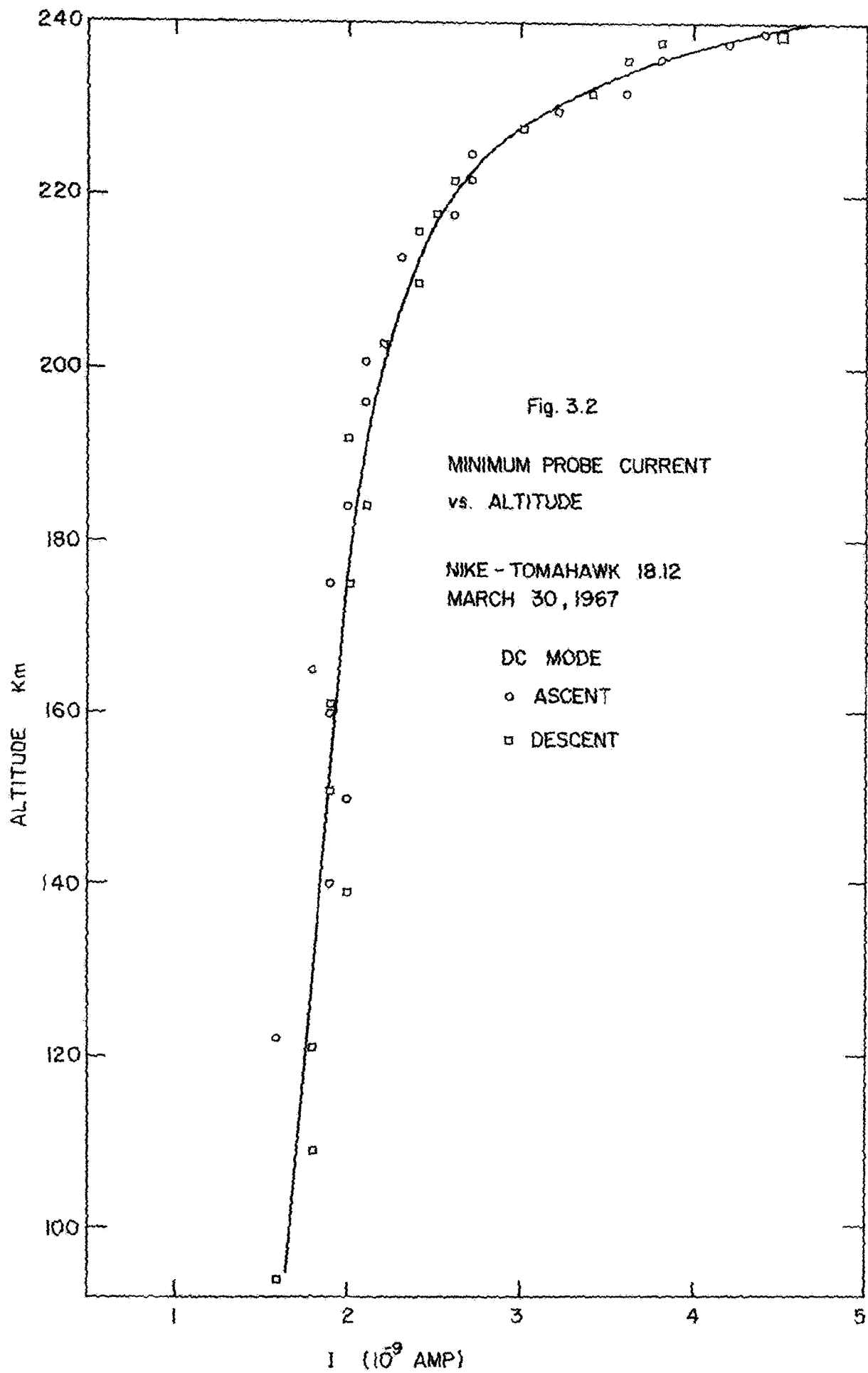
Table 3.2 MINIMUM PROBE CURRENT AND ELECTRON FLUX ($E \geqslant 15ev$)

	Altitude (km)	$I_R(10^{-9}A)$	$I_c(10^{-9}A)$	$I_R'(10^{-9}A)$	$J(10^8/cm^2-sec)$
Ascent	122	1.6	1.8	1.0	2.0
	140	1.9	1.2	1.0	2.4
	150	2.0	2.3	1.0	2.5
	160	1.9	1.6	1.4	2.4
	165	1.8	1.6	1.4	2.3
	175	1.9	1.7	1.0	2.4
	184	2.0	2.0	1.6	2.5
	196	2.1	2.0	1.6	2.6
	201	2.1			2.6
	213	2.3	2.3	2.0	2.9
	218	2.6	2.9	2.1	3.3
	222	2.7	3.3	2.6	3.4
	225	2.7	3.2	2.7	3.4
	232	3.6	4.1	3.3	4.5
	236	3.8	4.2	3.6	4.8
	238	4.2	4.3	4.2	5.3
	239	4.4	4.7	4.3	5.5
Descent	94	1.6			2.0
	109	1.8			2.3
	121	1.8	2.0	1.0	2.3
	139	2.0	2.5	1.3	2.5
	151	1.9	2.1	1.3	2.4
	161	1.9	2.0	1.4	2.4
	175	2.0	2.1	1.6	2.5
	183	2.1	2.0	1.7	2.6
	192	2.0	1.7	1.7	2.5
	195	2.1			2.6
	203	2.2	2.0	1.4	2.8
	210	2.4	2.6	1.9	3.0
	216	2.4	2.5	2.0	3.0
	222	2.6	2.4	2.2	3.3
	228	3.0	2.7	2.5	3.8
	232	3.4	3.0	3.0	4.3
	236	3.6	3.9	3.2	4.5
	238	3.8	4.1	3.5	4.8
	239	4.5	4.0	4.2	5.6

DC Mode
Nike-Tomahawk March 30, 1968

I_R, I_R' = Minimum probe current obtained from 10^{-9}, 10^{-8} A electrometer sensitivity, respectively

I_c = Constant for best exponential fit for secondary current

than approximately 15.5 ev. These measurements were obtained from the currents corresponding to the flat sections of the sweep. I_R was obtained when the electrometer was in the most sensitive range (10^{-9}A). Table 3.2 also contains the values measured using the next sensitivity (10^{-8}A) and indicate similar results. We have chosen the flat portion of the potential sweep so that the displacement current $\left(\propto \dfrac{dV}{dt} \right)$ is not a contributing factor. These measurements refer to the case where the probe was operated in the DC mode and as such, without information concerning the electron energy distribution for the energies greater than $\sim$ 15 ev, no conclusions can be drawn with regard to their exact concentration.

Figure 3.3 shows a typical section of the current curve as a function of the applied retarding probe potential with respect to the vehicle. This was obtained at an altitude of approximately 233 km on rocket ascent. The current appears to be relatively linear with applied potential for the retarding voltages in the range of 6-13.5 volts. For the lower altitudes, this linear section extended to smaller retarding potentials. Since the second derivative of the current in this range of retarding potentials is nearly zero from the Druyvesteyn relationship given by equation (2.18), we may conclude that there exists relatively very few electrons with energies between $\sim$ 8 and 15 ev. The current that is detected in this range of retarding potentials is primarily that due to electrons with energies > 15 ev. We shall designate this quantity as the residual probe current which can be expressed as:

$$i_R = I_0 + cV \quad , \tag{3.1}$$

where V is the retarding probe potential, I_0 is the "drift current"

Fig. 3.3

PROBE CURRENT vs. SWEEP POTENTIAL
~233 Km (18.12, ASCENT)
10^{-8} R SECTION, DC MODE

LEAST SQUARE LINEAR FIT (7-12 VOLTS)

SWEEP POTENTIAL (VOLTS)

PROBE CURRENT (10^{-8} AMPERES)
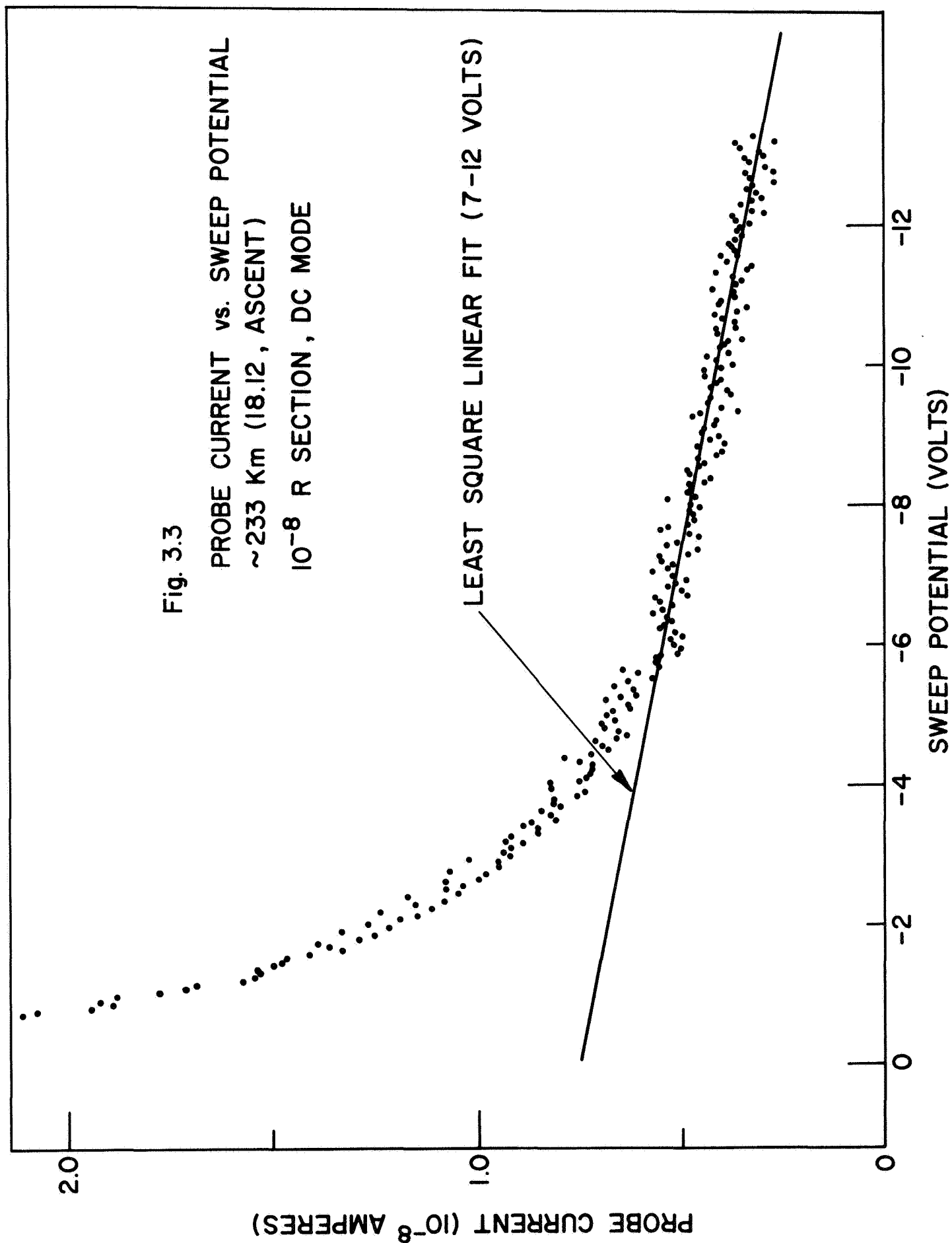
due to electrons with energies greater than ~ 15 ev, and $c = \dfrac{di_R}{dV}$,

the constant slope of the residual current. In terms of the

equilibrium energy distribution function F(E), they may be written

as:

$$I_o = \frac{n_o \bar{e v} A \alpha}{4} = \frac{A e \alpha}{2\sqrt{2m}} \int\limits_{E>15 \text{ ev}}^{\infty} F(E)E^{\frac{1}{2}} \, dE \qquad (3.2)$$

and (see Chapter II)

$$c = \frac{di_R}{dV} = - \frac{A e^2 \alpha}{2\sqrt{2m}} \int\limits_{E>15 \text{ ev}}^{\infty} F(E)E^{-\frac{1}{2}} \, dE \qquad , \qquad (3.3)$$

with A = effective collector area, e and m are the electronic charge

and mass, respectively, $\bar{v}$ is average speed of the electrons with

energies greater than 15 ev, and n_o is their concentration, i.e.,

$$n_o = \int\limits_{E>15 \text{ ev}}^{\infty} F(E) \, dE \ . \qquad (3.4)$$

The lower limits of these integrals do not in any way imply

that the energy distribution begins at or near 15 ev and was chosen

merely because it was the maximum retarding potential to which the

experiment was conducted.

Figures 3.4 and 3.5 show the experimental results obtained

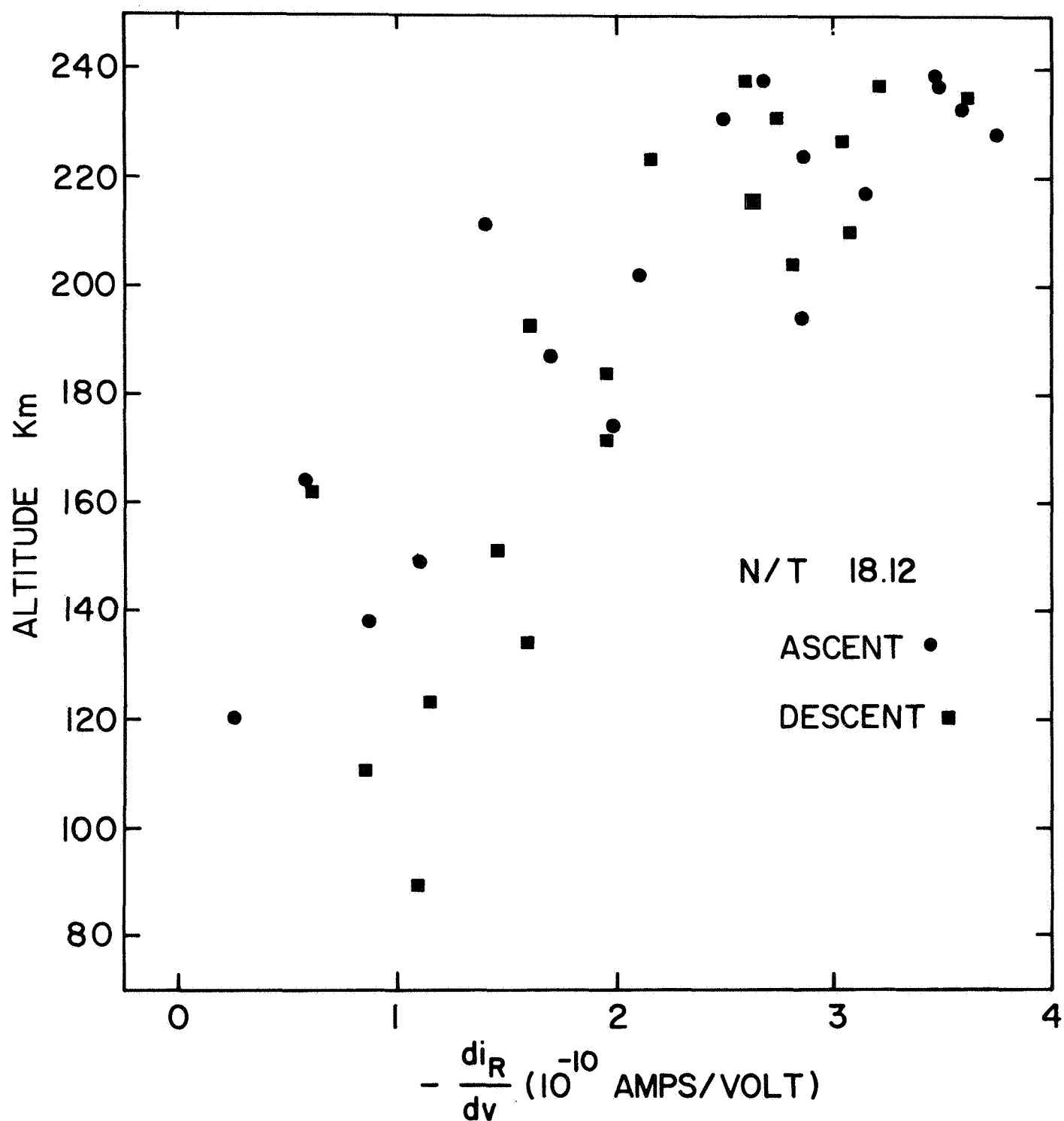for the values of c and I_o, respectively, as a function of altitude for

Fig. 3.4 RESIDUAL CURRENT SLOPES

N/T 18.12
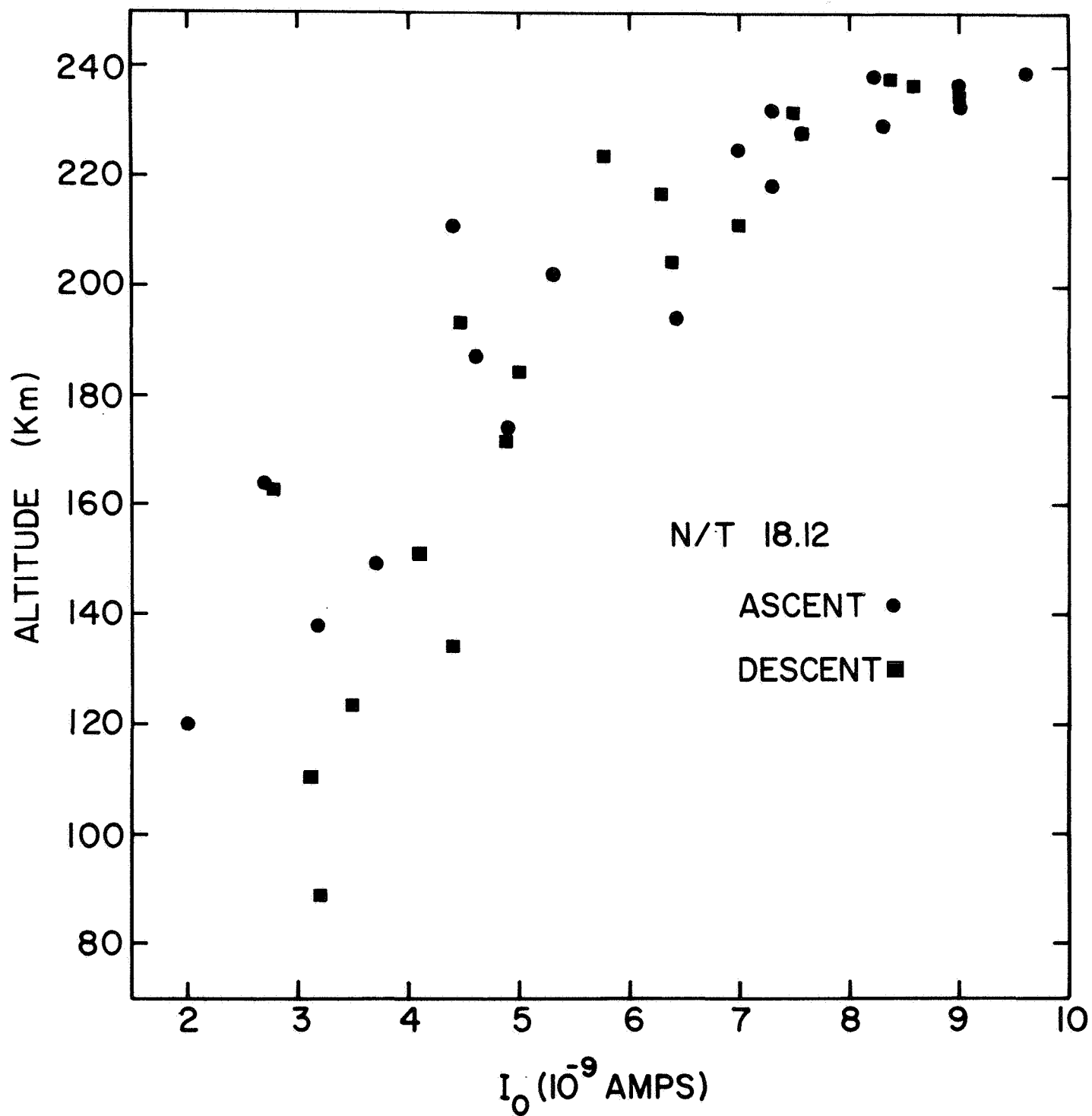
ASCENT ●

DESCENT ■

Fig. 3.5 i_R (V=O) vs. ALTITUDE

both payload ascent and descent. They were calculated from the current curves in the retarding probe potential range of 7 - 12 volts relative to the vehicle. The values for the slopes c were obtained by applying a least square routine to compute the best linear fits of the digital data. The values for I_o were obtained by extrapolating from the linear sections to plasma potential utilizing the values obtained for c and the vehicle potential data.

We note that there exists a very close correlation between Figures 3.2, 3.4, and 3.5 where each quantity as a function of altitude increased by a factor of three nearly simultaneously from approximately 120 to 240 km. It is as if the linear current i_R was being rotated about its intercept with the zero current axis. We shall discuss this particular point in more detail in the next chapter.

There appears to be excellent agreement between the upleg and downleg measurements of the minimum probe currents as shown in Figures 3.2. The measurements of the residual current slopes c, together with the extrapolated values for I_o (i_R for V = 0), were determined at a lower electrometer sensitivity (10^{-8}A) and as a result of the smaller signal to noise ratio, showed a great deal more scattering.

2. The Secondary Current

The residual probe current was defined in the preceeding section as the contribution from ambient electrons with energies E > 15 ev. By subtracting this quantity from the total probe current, we may then obtain the current contribution from ambient electrons whose energies are less than $\sim$ 15 ev. Since we observe nearly no

electrons in the range of energies between approximately 8 and 15 ev (i.e., the current is linear with the retarding probe potential approximately where the residual currents were computed), the contributions to the total probe current less the residual current are primarily from the ambient electrons with energies less than $\sim$ 8 ev. The slopes of the residual current from most of the curves are relatively small ($\sim$ 1 - 3 x 10^{-10} amps/volt) so that for all practical purposes, we are subtracting a constant term from the total probe current.

We shall call the current from the electrons with energies less than $\sim$ 8 ev, the reduced probe current. Figure 3.6 shows the reduced probe current as a function of the retarding probe potential plotted on log scale. This particular current-voltage characteristic was obtained at approximately 194 km on payload ascent. It is made up of three sections corresponding to three different levels of electrometer sensitivity ($10^{-6, -7, -8}$A).

Since the reduced current-voltage characteristic indicated two distinct linear regions when the current is plotted on a logarithmic scale, we shall treat this current as arising from two distinct distributions, a thermal and a secondary distribution. The section AB as shown in Figure 3.6 may be identified as the retarded thermal current and we shall refer to section BC as the retarded secondary current. The thermal current is generally observed to occur for probe potentials greater than $\sim$ 1 volt negative with respect to the plasma while the secondary current appears for probe potentials less than this value.

Fig. 3.6

REDUCED PROBE CURRENT vs.
SWEEP POTENTIAL (18.12, ASCENT)

A

RETARDED
THERMAL
CURRENT

194 Km

B

RETARDED SECONDARY
CURRENT

C
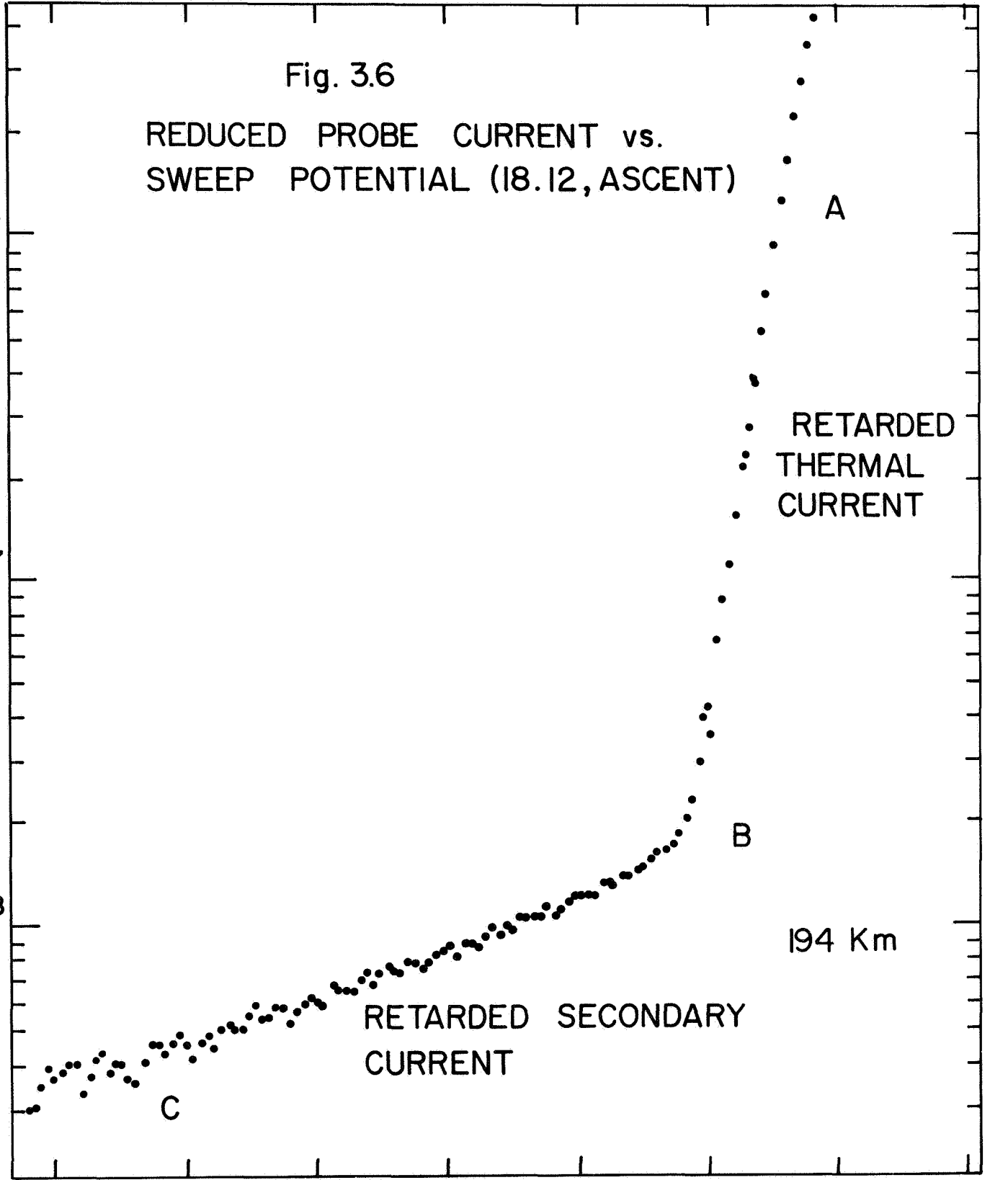
As was stated in Chapter II, the pulse probe current in the
DC mode of operation under a retarding probe potential relative to the
plasma has essentially the same current characteristic as the Langmuir
probe with the exception that there is no positive ion contribution to
the total collector current. The probe screens merely reduce the
transmission and alter the spatial potential variation about the
collector. The three outer elements of the probe are at approximately
the same potential. Thus, for a retarding sweep potential V, the
current is essentially independent of the exact potential variation
about the collector (for our particular case, the variation is
monotonic), and if the electrons have a Maxwellian distribution, the
probe current may be expressed as:

$$i(V) = \alpha\ I_0\ e^{\frac{-eV}{kT}}\ .$$

(3.5)

A plot of log i(V), as a function of the retarding potential V, will
then result in a straight line where the slope is inversely
proportional to the electron temperature.

The retarded thermal current shown as the section AB in
Figure 3.6 is indeed approximately a straight line and the majority
of the electrons that contribute to this current may be characterized
as having a Maxwellian energy distribution. The electron temperatures
calculated in terms of the slopes will be discussed in the following
section.

The results for the secondary probe currents are at first
glance somewhat unexpected in that they indicate the current as being
very nearly an exponential function (usually associated with a

Maxwellian distribution of energies) of the retarding probe voltage

over a rather extensive stretch of the curve. Furthermore, this

exponential form was found to be an excellent approximation for all

the curves that were obtained between the altitudes of $\sim$ 120 km and

240 km (the latter corresponding to payload apogee) in both payload

ascent as well as descent. Figure 3.7 shows three different reduced

probe current curves corresponding to three different altitudes

(126, 174, and 239 km).

The exponential slopes were found to generally decrease

with increasing altitudes and the magnitudes of the current corresponding

to a given retarding probe potential were observed to increase with

increasing altitudes. The exponential slopes of the secondary probe

currents were approximately 10 times smaller in general, in

comparison with the exponential slopes of the thermal current section.

In principle, the Druyvesteyn method can be applied for

obtaining the electron energy distribution function (equation 2.18)

by taking the second derivative of the current with respect to the

retarding sweep potential. However, graphical differentation is

inaccurate even for exceptionally high signal to noise ratios without

some "smoothing" of the curves. In this particular case, we have

concluded that this would be generally unnecessary since the retarded

secondary probe current is so nearly exponential. So, with respect to

data analysis of the secondary distribution current, we shall treat it

as if it represents a "second Maxwellian" distribution and determine

a temperature and density from each current characteristic in the same

manner that we shall treat the thermal current. We shall present these

Fig. 3.7

REDUCED PULSE PROBE CURRENT vs. SWEEP POTENTIAL

NIKE – TOMAHAWK 18.12
MARCH 30, 1967

DC MODE, ASCENT

$\triangle$ 10^{-6} R
$\square$ 10^{-7} R
$\bullet$ 10^{-8} R
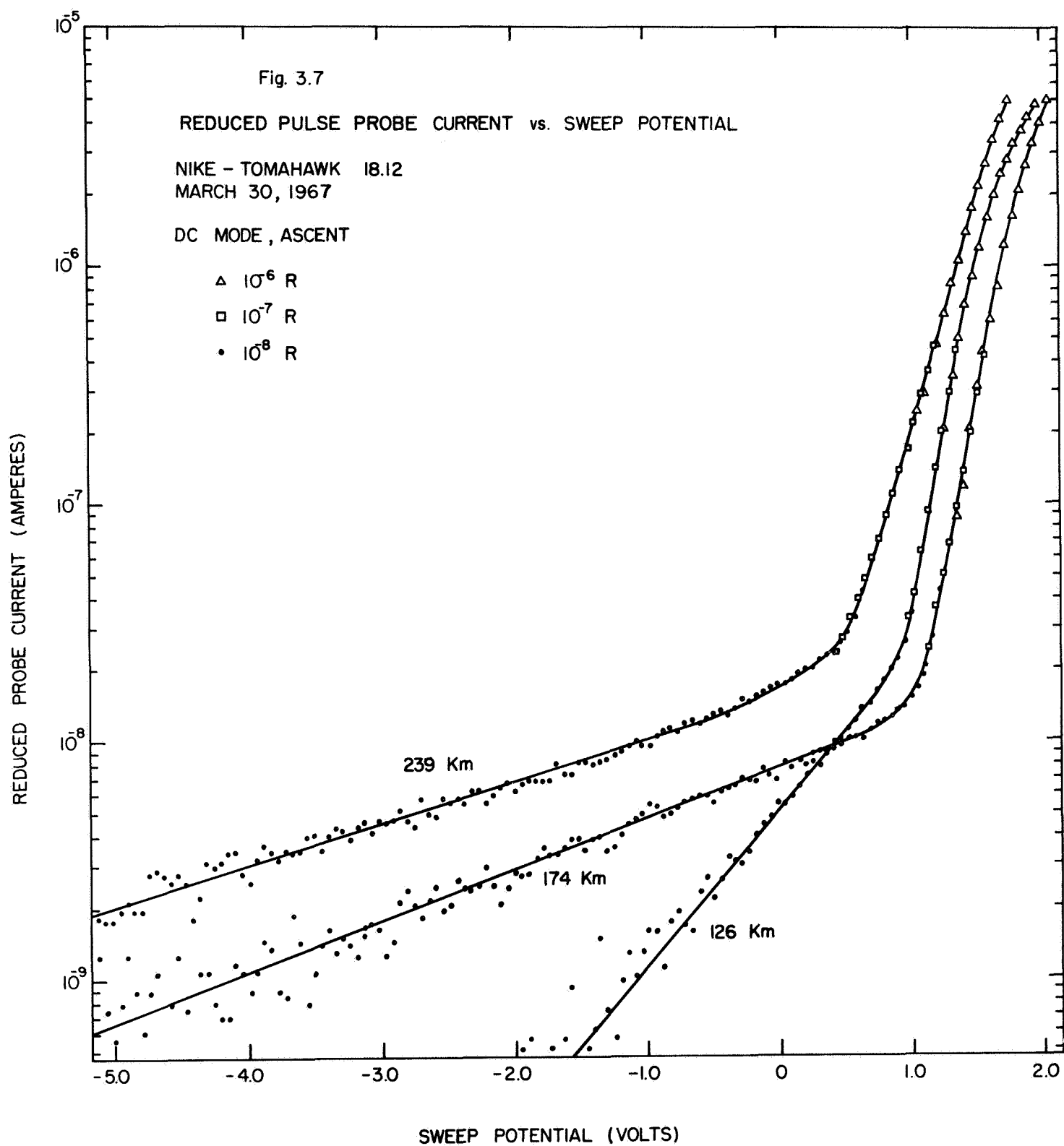
values together with their discussion in the next chapter.

3. The Thermal Current

Because the energy distribution of the thermal electrons is approximately Maxwellian, the retarded thermal current when plotted logarithmically as a function of the probe potential gives rise to a straight line with the temperature of the electrons being inversely proportional to the exponential slope:

$$T = \frac{\left(\frac{e}{k}\right)}{\left|\frac{d(\ln I)}{dV}\right|} \qquad (3.6)$$

If we determine the electron temperature from the current curve where the electrometer had a fixed sensitivity, then it matters not what exact value we had for the sensitivity provided that it was constant over the time period when the current was measured. The resulting temperature does, however, depend on the zero current level.

The exponential slopes of the current from the retarded thermal section of the curves were obtained by making least square fits (with weighted residuals) of the digitized data . The results for the thermal electron temperature, as determined with equation (3.6) are shown as a function of the altitude in Figure 3.8, both for payload ascent and descent.

As the retarded probe potential is made less negative with respect to the plasma, the collector current as a function of the probe to plasma potential begins to deviate from the exponential form at or near the plasma potential. When the probe is under an accelerating potential with respect to the plasma, the current is, in general, a

Fig 3.8

RAW THERMAL ELECTRON TEMPERATURES vs. ALTITUDE (18.12)

● ASCENT

■ DESCENT

ALTITUDE Km.

THERMAL ELECTRON TEMPERATURE 10^3 °K
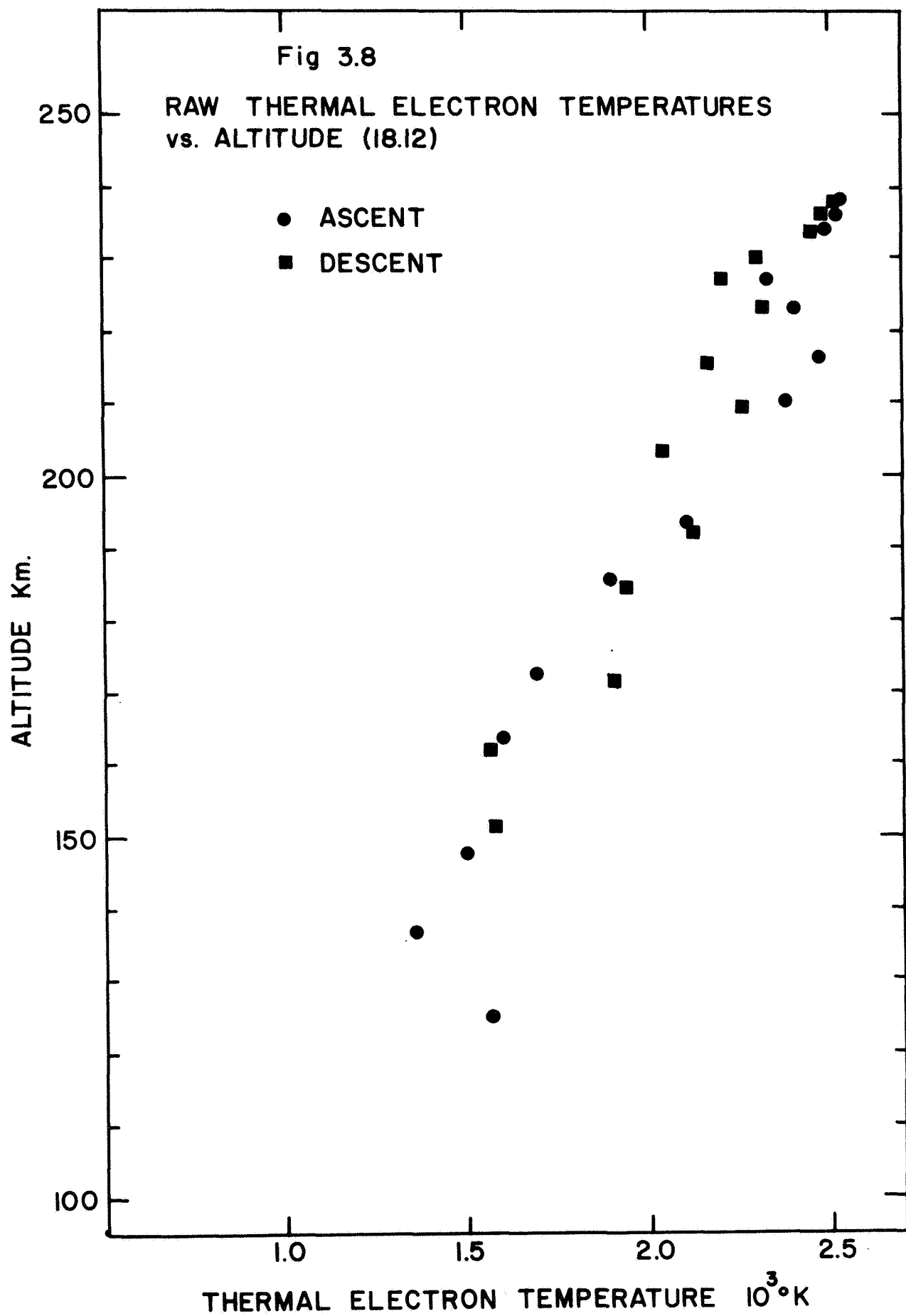
function of the dimension of the sheath associated with the probe and will vary more gradually with probe potential than the exponential variation in the retardation region. The location of the point corresponding to plasma potential on a Langmuir probe characteristic is, in general, very difficult to ascertain. Even if the "break point" on the logarithmic current plot is clearly identifiable (in most cases they are not sharp), this inflection point need not correspond exactly to plasma potential. The form of the current near plasma potential is strongly dependent upon the surface patch effect of the collector. However, this patch effect does not apply to the pulse probe current because of the large potential bias present between the innermost grid (which is the effective collection area) and the collector.

In the pulse probe experiment aboard flight 18.12, the failure of the probe erection mechanism left the probe in a position to be effected by the sheath associated with the vehicle, thus, the current deviates from the exponential form at a slightly negative potential with respect to the plasma. The shielding effect of the vehicle sheath may or may not have effected the entire field of view of the probe. Nevertheless, the conclusion is that we observe a net reduction of the thermal current beginning at a point slightly negative of the plasma potential and shall abandon any attempt to utilize the thermal current for deriving ambient electron densities.

With regard to obtaining vehicle potentials, we have utilized ionosonde electron densities provided to us by J. W. Wright, Figure 3.10. The method that was employed is as follows: first, we extend the retarded thermal current which appears as approximately a straight line on the

Fig. 3.10

IONOSONDE ELECTRON
CONCENTRATION

TAKEN AT TIME OF
N/T 18.12 LAUNCH
(MARCH 30, 1967)
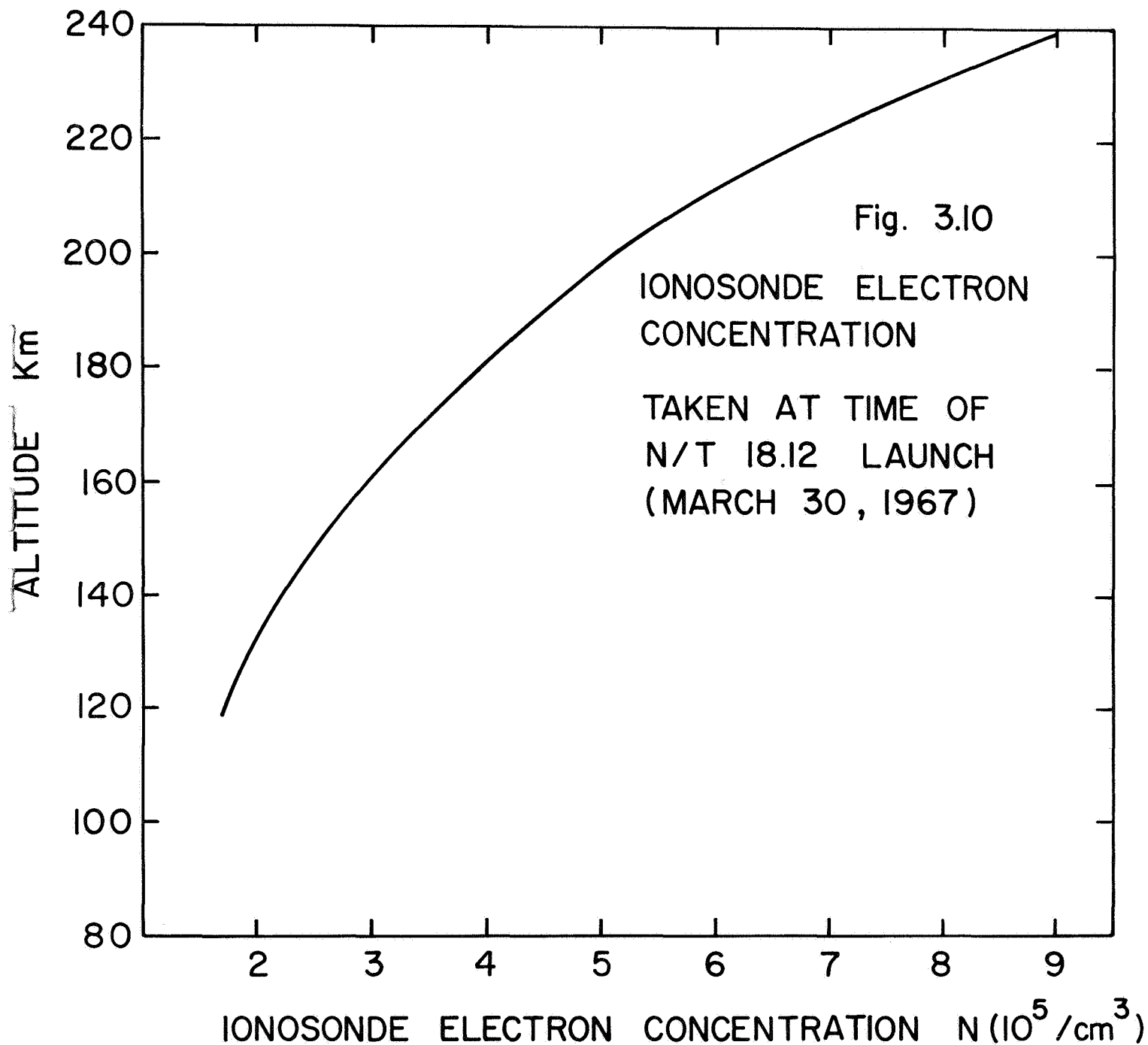
semilog plot, toward more positive potentials. Then, computing for

the drift current I_o by:

$$I_o = \alpha n e A \sqrt{\frac{kT}{2\pi m}} \quad ,$$

where α = transmission coefficient, A = effective collector area (the

area of the innermost grid), T = electron temperature obtained by the

methods outlined above, and n = the ionosonde electron concentration,

we locate on the extended line the point corresponding to I_o. The

applied potential corresponding to this point is then equal to the

negative vehicle potential. We have plotted the values for the vehicle

potentials obtained in this manner as a function of altitude in

Figure 3.9, and shall leave their discussion to the following chapters.

Fig. 3.9

VEHICLE POTENTIAL vs. ALTITUDE
18.12
PULSE PROBE
• ASCENT
× DESCENT

VEHICLE POTENTIAL (VOLTS)
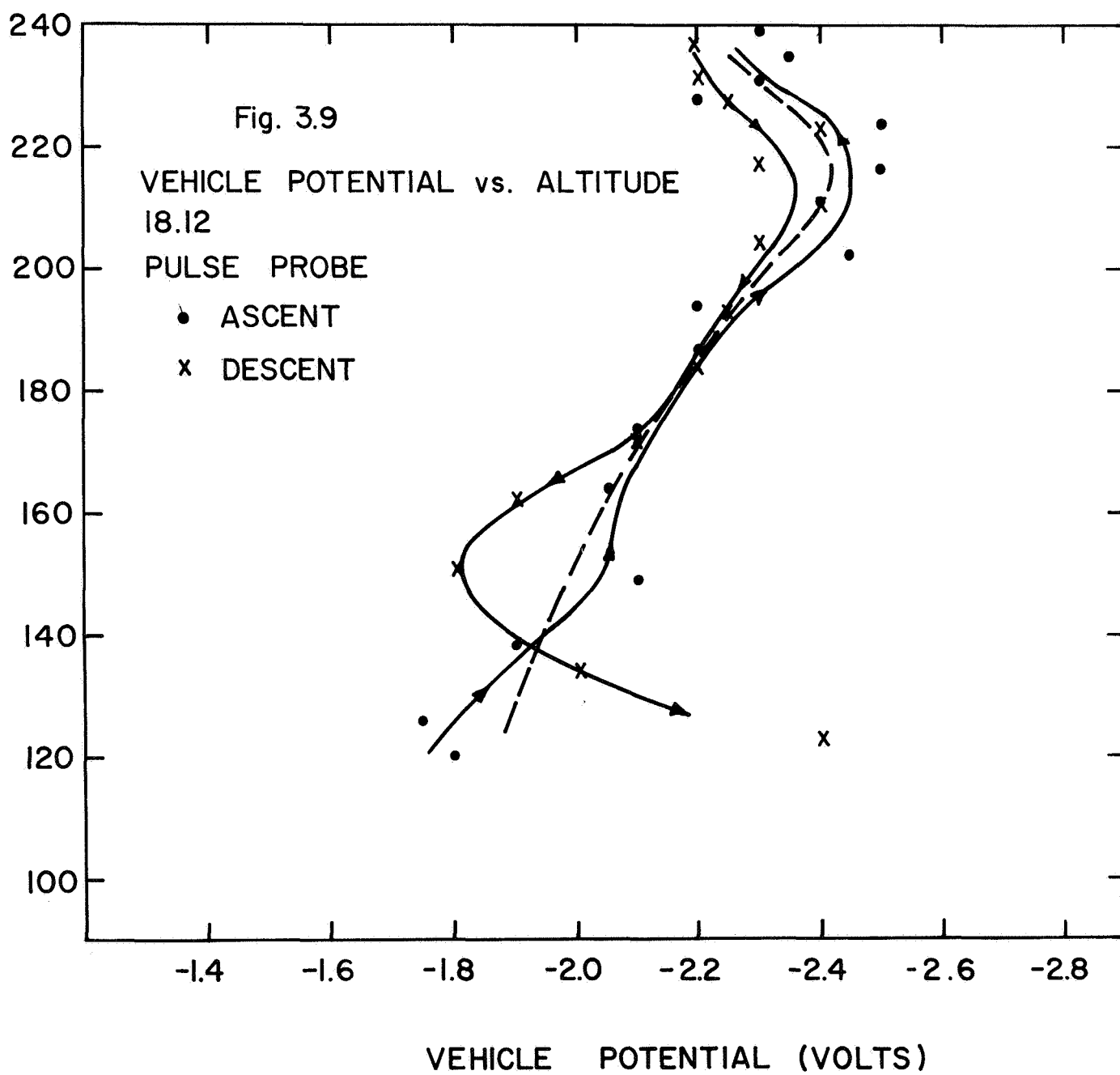
CHAPTER IV

ANALYSIS OF THE SUPRATHERMAL COMPONENT

A. Introduction

The experimental data, as obtained with the pulse probe operated in the DC mode, indicated that the total probe current can be considered as the sum of three distinct currents, each dominating over a separate region of retarding probe potentials. In our analysis, we attribute these observed currents to distinctly different electron distributions and have proceeded to analyze each term separately.

The collector current at small retarding probe potentials (⸴ less than 1 volt) is dominated, for the most part, by the collection of thermal electrons with a characteristic Maxwellian distribution of energies. The experimentally determined thermal temperatures were presented in the preceding chapter and were found to increase with altitude in the region between 120 to 240 km from approximately a value of 1.5 to 2.5 x 10^3 ^{o}K.

In this chapter, we wish to present the results from the analysis of the collector current detected with retarding probe potentials greater than approximately 1 volt, referring to this current as that produced by suprathermal electrons (i.e., electrons with energies greater than $\sim$ 1 ev). This suprathermal current is the sum of the linear residual probe current which is due to electrons with energies E > 15 ev, and what we have called the secondary current arising from a secondary distribution, that is, electrons with energies in the range between approximately 1 and 8 ev.

We have shown that the experimentally measured secondary current

is approximately an exponential function of the retarding probe potential

for the altitude region between approximately 120 to 240 km (payload

apogee). In the data analysis of the secondary currents, we compute

temperatures and densities based on the assumption that the secondary

distribution is Maxwellian. This is done with the understanding that

these derived parameters describe the exponential slopes of the

secondary currents and their intercepts at plasma potential, as there

exists no physical justification for the secondary distribution to be

Maxwellian (as there exists, for instance, in the case of the thermal

electrons).

The data analysis that we undertake for the secondary currents

are, therefore, very much simplified and in fact, identical to that

employed for the thermal currents with the exception that density

calculations were not possible for the latter on the 18.12 data for the

reasons given previously. The densities for the secondary distribution

were obtained from the drift currents which were derived by exponentially

extrapolating the secondary currents to plasma potential. For this, we

have made use of the vehicle potentials that were obtained in the

preceding chapter.

In section C of this chapter, we will present the results obtained

from an analysis of the linear probe residual currents assuming that the

energy distribution for the electrons with energies greater than $\sim$ 15 ev,

is approximately monoenergetic. Although this may be a gross

simplification of the actual situation, it nevertheless serves the

purpose of illustrating that the increases observed for the residual

probe currents as altitude increases can be primarily attributed to an

increase in the concentration of the high energy component (E $\gtrsim$ 15 ev).

B. The Secondary Distribution

    1. Temperatures

        The exponential slopes of the secondary current were determined in approximately the same manner in which the thermal currents were analyzed (Chapter III). Here, of course, we are dealing instead with the total collector current less the residual current for retarding probe potentials approximately greater than 1 volt. The exponential slopes of the secondary current were obtained by making least square fits (with weighted residuals) of the digitized data. The electron temperatures corresponding to the secondary energy distribution were obtained from the exponential slopes utilizing equation (3.6).

        In Figure 4.1, we have plotted the temperatures for the secondary distribution as a function of altitude for both payload ascent and descent. The values for the temperature T_s generally increased with increasing altitude, the largest gradient occurring between approximately 150 to 170 km. Between roughly 130 km to 240 km, T_s increased by approximately a factor of three from $\sim$ 1 to $\sim$ 3 x 10^4 °K. Comparing the temperatures between payload ascent and descent, we find that they are in good agreement.

        These temperatures were obtained from the currents detected when the electrometer was operated in the 10^{-8}A scale. Thus, they are essentially independent of the exact value of the electrometer sensitivity provided that it was constant over the probe sweep. They are also independent of the transmission coefficient of the probe since the temperature is inversely proportional to the exponential slope of

SECONDARY
TEMPERATURE-ALTITUDE

NIKE TOMAHAWK 18.12

MARCH 30,1967

ASCENT ●
DESCENT ■

DC MODE, 10^{-8} R
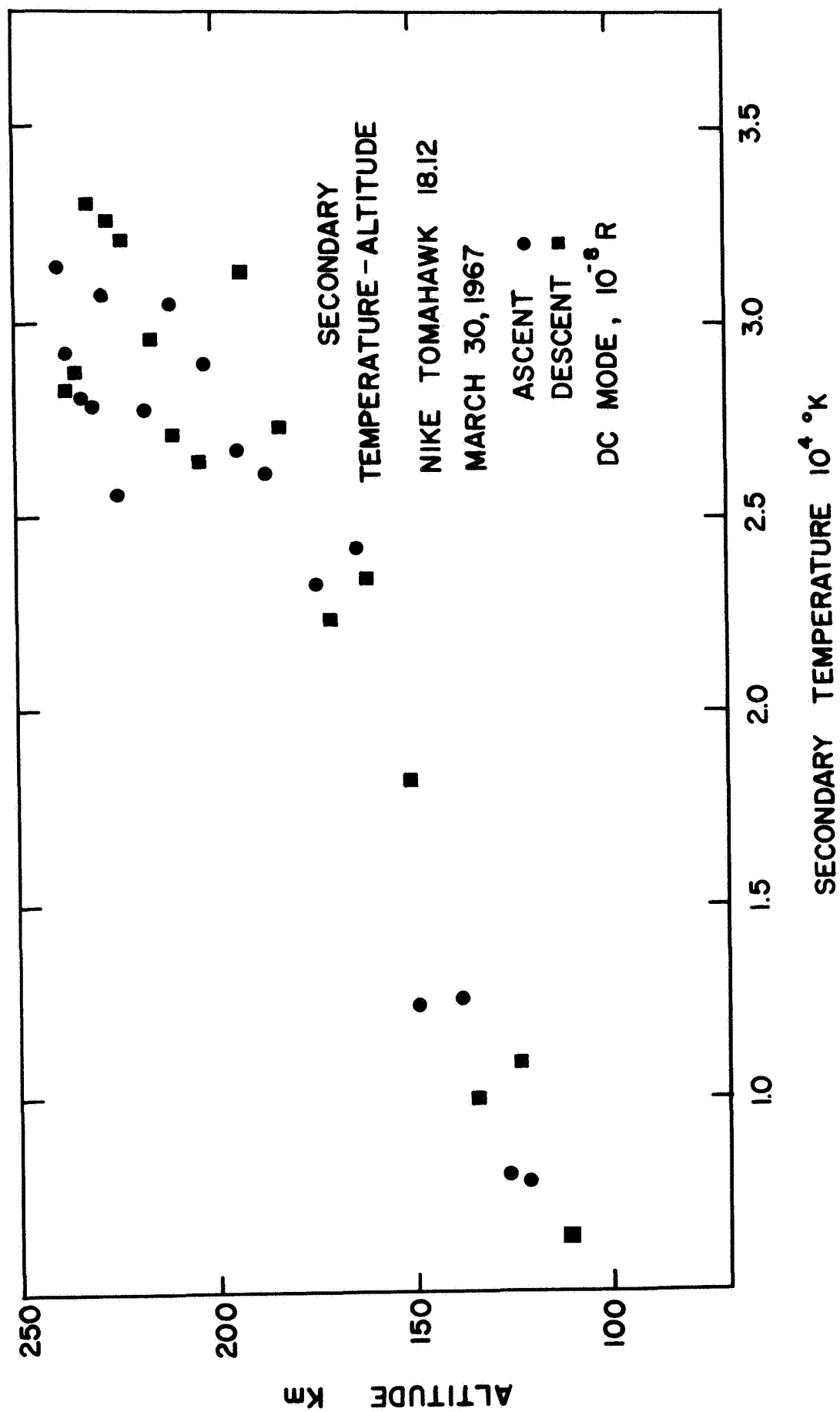
FIG. 4.1

the current. The number of data points obtained from the digitization was much greater than that obtained for the thermal section since the secondary current slopes were generally a factor of ten smaller.

In obtaining the secondary current from the total collector current, we have approximated the residual current by a constant rather than a linear function of the retarding probe potential. Since the slopes of the residual currents were relatively small at all altitudes, this amounted to only a small correction term to the total secondary current. The constant was determined by taking the average current corresponding to the retarding probe potential in the range of approximately 9 - 12 volts. It was found that this constant corresponded very closely to that providing the exponential fit with the lowest standard deviation ($\lesssim \pm$ 3% for the exponential slopes).

If we had utilized the second derivative of the current for determining the energy distribution function (i.e., following the Druyvesteyn method), then the subtraction from the total probe current of any constant term or any linear function of the retarding probe potential would not in principle alter the resulting distribution function in any manner whatsoever. But, since we are calculating the temperature [equation (3.6)] from the logarithmic derivative of the current $\left(\frac{dI}{I}\right)$, rather than from its second derivative, any large current offset will have an effect on the resulting temperature. However, from the result that the residual probe current does indeed provide the best exponential fit for the secondary current for all practical purposes, then any instrumental offset in the total probe current must appear only in the residual probe current and not in the exponential secondary current, i.e., the secondary current is an exponential function of the

retarding probe potential.

If we take for the secondary current as an exponential function of the retarding probe potential extending to the plasma potential, we may then apply corrections to the thermal temperatures by first subtracting from the total probe current the exponential extension of the secondary current. Then, from the corrected thermal currents, obtain the best fitted exponential slopes and new thermal temperatures using equation (3.6). These so-called corrected values of the thermal electron temperature are shown in Figure 4.2. The corrections are toward smaller values for the thermal temperature and generally amount to approximately 100 to 200°K. Thus, the corrected thermal electron temperatures are of the order of ten times smaller than the temperatures derived for the secondary distribution. The effect of the residual probe current is completely negligible for thermal current corrections.

2. Concentrations

The assumption of a Maxwellian energy distribution function for the secondary electrons allows us to make some estimates concerning their total concentrations. The expression for the drift current corresponding to the probe being at plasma potential may be expressed as:

$$I_{os} = \alpha \; n_s \; e \; A \; \sqrt{\frac{kT_s}{2\pi m}} \quad , \tag{4.1}$$

where α = transmission coefficient, n_s and T_s are the concentration and temperature, respectively, for the secondary distribution.

Table 4.1 lists the values of n_s and the various parameters used in its determination. The vehicle potentials were obtained by the

Fig. 4.2

CORRECTED THERMAL
ELECTRON TEMPERATURE
18.12
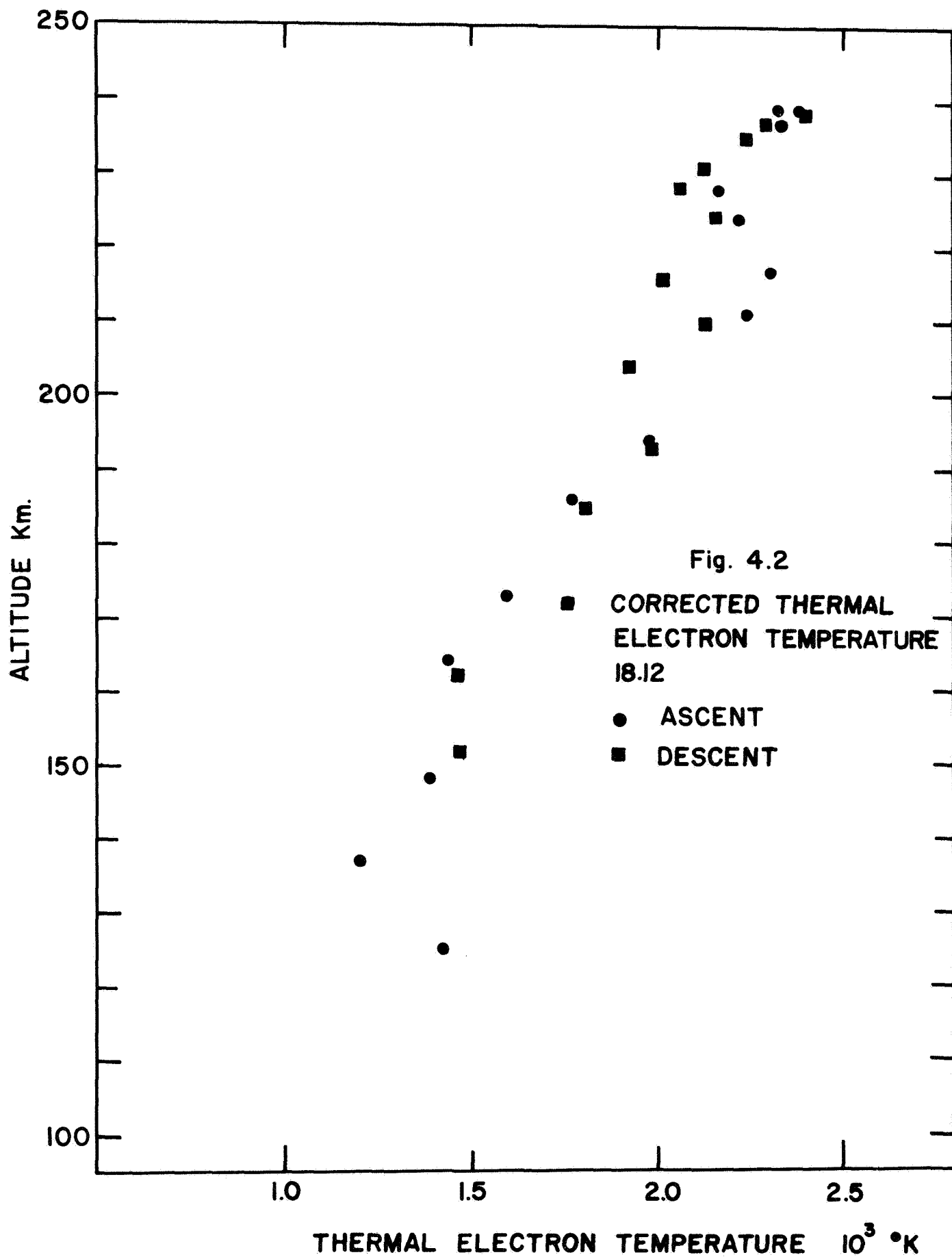
● ASCENT
■ DESCENT

TABLE 4.1 SECONDARY ELECTRON CONCENTRATIONS

	Altitude (km)	n_t(ionos.) $10^5/cm^3$	$I_o(10^{-6}A)$	V_s	$I_{os}(10^{-8}A)$	$n_s(10^2/cm^3)$	$f = \dfrac{n_s}{n_t}$ $(10^{-\cdot})$
Ascent	120	1.78	7.0	1.8	5.12	5.8	.33
	126	1.78	7.0	1.7	7.21	8.1	.46
	138	2.11	8.3	1.9	3.35	3.0	.14
	149	2.57	10.6	2.1	2.93	2.4	.09
	164	3.11	15.0	2.1	2.09	1.5	.05
	174	3.58	18.4	2.1	2.14	1.4	.04
	187	4.24	23.6	2.2	2.28	1.4	.03
	194	4.75	27.1	2.2	2.60	1.6	.03
	202	5.17	30.2	2.5	2.33	1.4	.03
	211	6.01	35.1	2.4	2.51	1.4	.02
	217	6.46	37.7	2.5	2.70	1.6	.02
	224	7.31	42.7	2.5	2.88	1.6	.02
	228	7.70	45.9	2.2	2.51	1.5	.02
	231	8.13	48.5	2.3	2.98	1.8	.02
	235	8.40	50.1	2.4	3.26	1.9	.02
	237	8.80	52.5	2.2	3.63	2.1	.02
	239	9.00	53.7	2.3	4.08	2.4	.03
Descent	237	8.80	52.5	2.2	3.63	2.1	.02
	231	8.13	48.5	2.3	2.88	1.6	.02
	227	7.60	45.3	2.3	2.42	1.4	.02
	223	7.20	42.0	2.4	2.5	1.5	.02
	216	6.34	37.0	2.3	2.5	1.5	.02
	210	5.85	34.1	2.4	2.37	1.4	.02
	204	5.32	31.0	2.3	2.5	1.5	.03
	193	4.70	26.8	2.2	2.5	1.5	.03
	184	4.10	22.2	2.2	2.42	1.5	.04
	171	3.50	17.4	2.1	2.33	1.5	.04
	162	3.08	14.8	1.9	1.86	1.3	.04
	151	2.73	11.3	1.8	2.23	1.8	.07
	134	1.90	7.5	2.0	3.90	3.6	.19
	123	1.78	7.0	2.4	10.9	11.5	.65

Nike-Tomahawk 18.12 March 30, 1968
DC Mode

I_o = Thermal drift current

I_{os} = Secondary drift current

V_s = Vehicle potential

α = 0.8

extrapolation of the thermal current section toward positive probe

potentials and then utilizing ionosonde densities for locating the

point corresponding to plasma potential as outlined in the previous

chapter. The values obtained for n_s are approximately constant over

the range of altitudes between approximately 150 to 240 km, the latter

corresponding to payload apogee. In this range of altitudes, the

secondary concentration is approximately 150 - 200 electrons/cm^3 for

$\alpha \sim 0.8$.

We note that because the secondary currents possess much

smaller exponential slopes than the thermal currents, the

uncertainties of the vehicle to plasma potential are much less likely

to produce significant errors in the values obtained for the secondary

drift currents I_{os} and therefore, in the secondary concentrations.

This is especially true at the higher altitudes where the temperatures

of the secondary distribution are approximately 3×10^4 $^\circ K$.

C. <u>Electrons with Energies $\overset{>}{\sim}$ 15 ev</u>

It was noted in the preceding chapter that in the negative range

of applied probe potentials of approximately 6 - 13 volts with respect

to the vehicle (or, approximately 8 - 15 volts with respect to the

plasma), the collector current was observed to be linear with the

retarding probe potential. From the Druyvesteyn relationship, it

was then concluded that there exists few electrons with energies

between roughly 8 and 15 ev (since $\dfrac{d^2 i}{dv^2} \sim 0$ in this region of retarding

potentials).

Furthermore, this linear current, which we have called the residual

probe current, was attributed to ambient electrons with energies

greater than $\sim$ 15 ev and was subtracted from the total collector current in the analysis of the temperatures and concentrations of the secondary distribution. The slopes of the residual probe current and their intercepts at plasma potential were presented in Chapter III (Figures 3.4 and 3.5).

We attribute the detected residual probe currents to the existence of a high energy component of ambient electrons (E $\stackrel{>}{\sim}$ 15 ev). It is unlikely that this current is the result of photoelectric or secondary emission of electrons from the collector because such a current would appear as a positive current to our detector. The large positive potential bias on the collector ($\sim$ 26 volts) relative to the innermost grid would suppress any significant electron emission from the collector element. Displacement currents associated with the probe sweep are small ($< 2 \times 10^{-10}$ AMPS), and again of the opposite sign to the observed residual probe current (in the DC mode of operation, the probe sweep is toward more negative values.) The overall effect of the displacement current is approximately a constant term rather than a linear function of the retarding potential (i.e., $I_D \propto \frac{dV}{dt}$, and for the linear probe sweep, $\frac{dV}{dt}$ is approximately constant). Thus, both of these effects contribute to produce small positive correction terms ($< 10\%$) to the observed residual probe current.

Since the maximum negative probe potential relative to the plasma was approximately 15 volts, we do not have any information regarding the energy distribution for the electrons with energies beyond $\sim$ 15 ev. In the absence of experimental data concerning this distribution, we shall assume for the present that the high energy component (E $\stackrel{>}{\sim}$ 15 ev)

was approximately monoenergetic with energy E_0. This is equivalent to assuming that the current continued to vary linearly with the retarding probe potential up to $V_0 = E_0/e$, and remained zero thereafter.

If we take for the energy distribution function $F(E)$ to be a δ-function, then equations (3.2) and (3.3) may be reduced to:

$$I_0 = i_R(V = 0) = \frac{\alpha A e}{2\sqrt{2m}} n_0 E_0^{\frac{1}{2}}$$ (4.2)

for the drift current, and

$$c = \frac{di_R}{dV} = -\frac{\alpha A e^2}{2\sqrt{2m}} n_0 E_0^{-\frac{1}{2}}$$ (4.3)

for the slope of the residual current.

Solving for E_0, we obtain

$$E_0 = -\frac{e I_0}{c} \quad .$$ (4.4)

If V_0 corresponds to the retarding probe potential where the linear residual current intercepts the zero current axis, i.e., $i_R(V_0) = I_0 + c V_0 = 0$, then $E_0 = e V_0$. The electron concentration n_0 of this high energy component can be obtained from either equation (4.2) or (4.3), once E_0 is known.

In Figure 4.3, the computed values for E_0, as determined with equation (4.4) with the experimentally measured values of the residual probe current, are plotted as a function of altitude for both payload ascent and descent. With the possible exception of the two points occurring at approximately 160 km, the values for E_0 are relatively constant ($\sim$ 26 ev). It is not clear why the large departure (by

Fig 4.3

E_0 vs. ALTITUDE

18.12
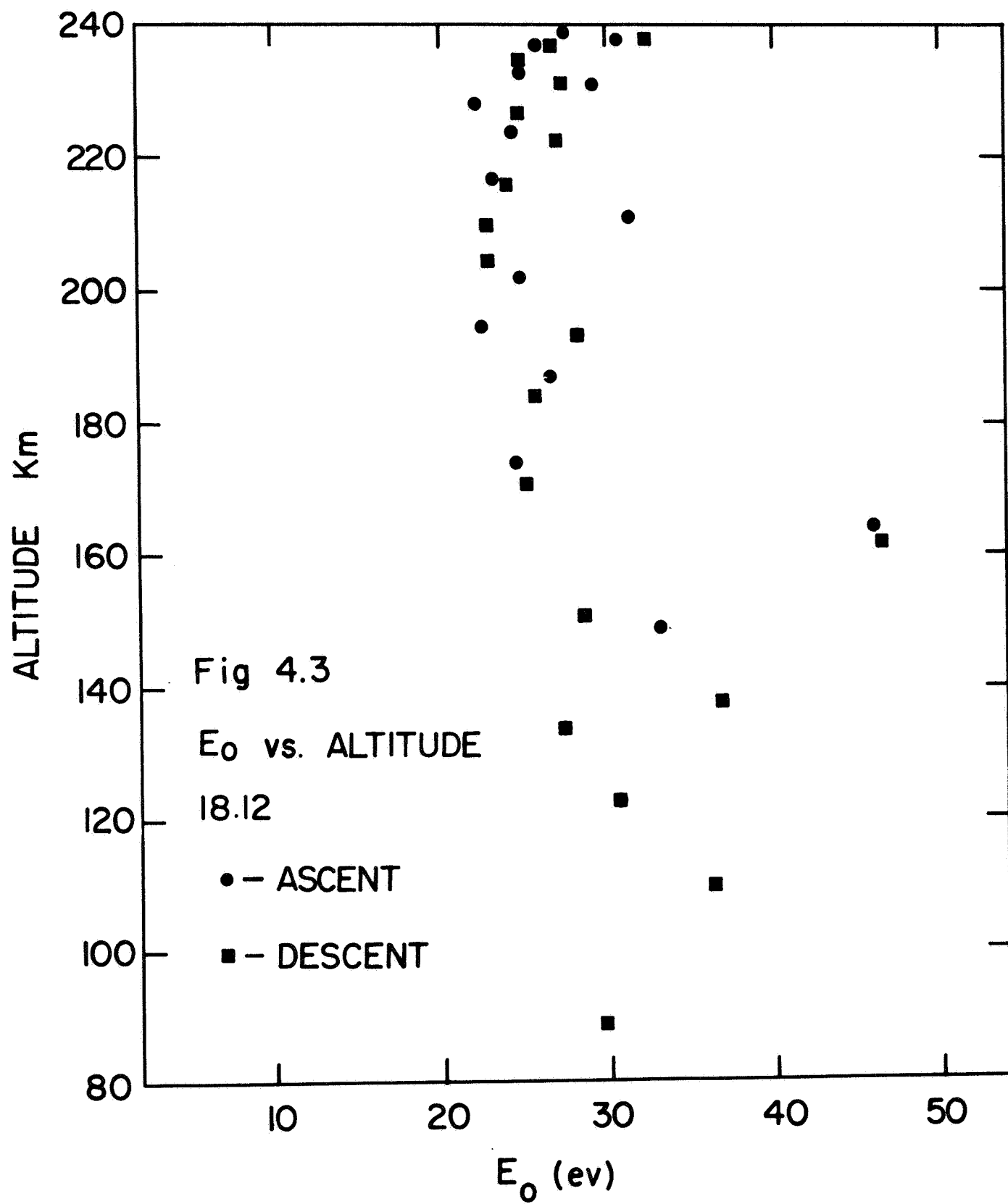
● — ASCENT

■ — DESCENT

almost a factor of two) occurs at approximately 160 km, on both ascent
and descent, with roughly the same deviation.

The values for the electron concentration n_o, based on the
assumption of a monoenergetic distribution, are shown as a function of
altitude in Figure 4.4 for both payload ascent and descent. There is
a general increase with increasing altitude by roughly a factor of
three from $\sim$ 5 to 14 electrons/cm^3, between approximately 120 to 240 km.

Thus, under the assumption that the energy distribution for
electrons with energies greater than $\sim$ 15 ev is monoenergetic, the
increases that are observed for the residual probe currents can be
attributed to the increase in the concentration n_o. We note that the
values for E_o are independent of the coefficient of transmission of the
probe and the electrometer sensitivity, assuming that they are
approximately constant over a particular probe sweep. The concentration
n_o, on the other hand, depends on both of these quantities and in the
expressions that we have utilized, it is only weakly dependent upon
the value of E_o [the inverse half power in equation (4.2), or directly
as the half power in equation (4.3)].

For an arbitrary energy distribution function defined over the
range of energies between E_1 and E_2, then it is clear that $E_1 < E_o < E_2$,
where $E_o \sim$ 26 ev for the altitude region between approximately 160 to
240 km. Writing for the energy distribution function F(E) as:

$$F(E) = n_o \ f(E) \ ,$$

where n_o is the concentration for electrons with energies greater than
$\sim$ 15 ev, we obtain the following expressions for the residual probe
current:

Fig. 4.4

n_0 vs. ALTITUDE

18.12

ASCENT ●

DESCENT ■
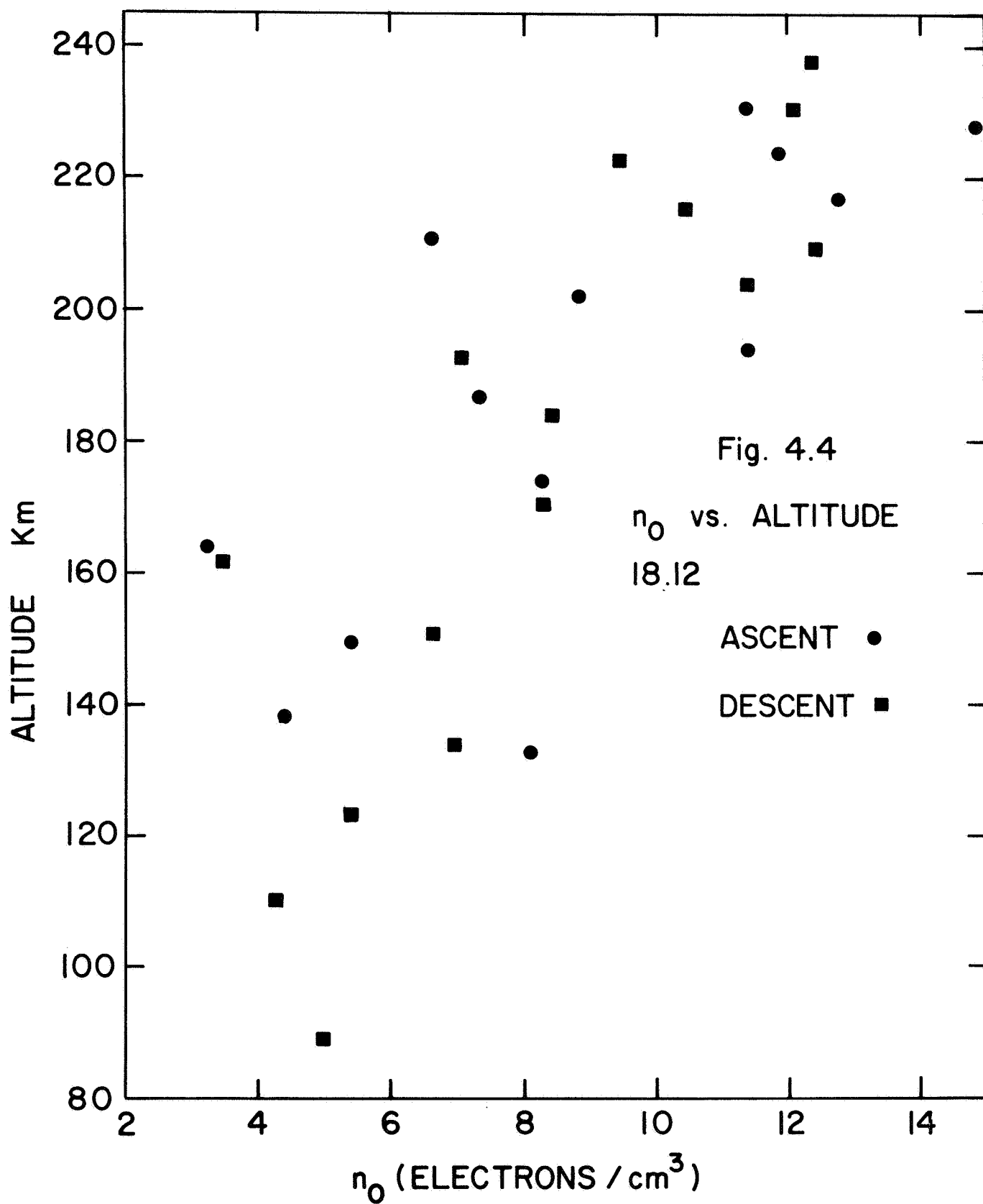
$$I_o = \frac{Ae\alpha}{2\sqrt{2m}} \; n_o \int_{E_1}^{E_2} f(E)E^{\frac{1}{2}}dE \qquad (4.5)$$

and

$$c = - \frac{Ae^2\alpha}{2\sqrt{2m}} \; n_o \int_{E_1}^{E_2} f(E)E^{-\frac{1}{2}}dE \qquad (4.6)$$

If the distribution function $f(E)$ remained constant in the altitude range of ~ 160 to 240 km, then the observed increases in the residual probe currents must necessarily be due to the increases in the electron concentration n_o, since the integrals appearing in equations (4.5) and (4.6) are merely constants. It is also apparent that the simultaneous increases by a factor of three of the quantities I_o and c with altitude cannot be due to a lateral shift of the energy distribution function along the energy axis. For instance, if the lateral shift of $f(E)$ was toward greater energies, then the integral in equation (4.5) would increase because of the weighting factor $E^{\frac{1}{2}}$, whereas the integral in equation (4.6) involving the factor $E^{-\frac{1}{2}}$ would decrease. If the lateral shift was toward lower energies, we would encounter the same results with the roles played by the integrals being reversed.

Table 4.2 summarizes the results obtained assuming a monoenergetic distribution for the electrons with energies greater than ~ 15 ev. The last column in this table gives the integral flux of electrons with energies $\gtrsim 15$ ev. This was obtained by taking I_o, the drift current (Figure 3.5), and dividing it by eA. They indicate a general increase with altitude from $\sim 4 \times 10^8$ electrons/cm^2 - sec. at approximately 138 km to $\sim 1.2 \times 10^9$ electrons/cm^2 - sec. near 240 km.

Table 4.2 EFFECTIVE HIGH ENERGY E_o AND CONCENTRATION n_o

	Altitude (km)	$\frac{di_R}{dV}$ (10^{-9}A/V)	I_o (10^{-9}A)	E_o (ev)	n_o (cm^{-3})	J_o $(10^9/\text{cm}^2\text{-sec})$
Ascent	138	-.087	3.2	36.8	4.4	0.40
	149	-.111	3.7	33.1	5.4	0.46
	164	-.058	2.7	46.0	3.3	0.34
	174	-.198	4.9	24.6	8.3	0.61
	187	-.170	4.6	26.7	7.4	0.57
	194	-.285	6.4	22.4	11.4	0.80
	202	-.213	5.3	24.9	8.8	0.67
	211	-.140	4.4	31.4	6.6	0.55
	217	-.315	7.3	23.3	12.8	0.91
	224	-.286	7.0	24.4	11.9	0.87
	228	-.375	8.3	22.2	14.9	1.04
	231	-.249	7.3	29.4	11.4	0.91
	233	-.359	9.0	25.0	15.1	1.12
	237	-.348	9.0	25.9	15.0	1.12
	239	-.266	8.2	20.8	12.4	1.02
	239	-.348	9.6	27.7	15.4	1.20
Descent	239	-.259	8.4	32.4	12.4	1.05
	237	-.321	8.6	26.8	14.0	1.07
	235	-.361	9.0	25.0	15.2	1.12
	231	-.274	7.5	27.4	12.1	0.94
	227	-.305	7.6	24.8	12.8	0.95
	223	-.216	5.8	27.0	9.5	0.72
	216	-.263	6.3	24.1	10.9	0.79
	210	-.308	7.0	22.8	12.4	0.87
	204	-.282	6.4	22.8	11.4	0.80
	193	-.160	4.5	28.1	7.1	0.56
	184	-.195	5.0	25.7	8.4	0.62
	171	-.196	4.9	25.2	8.3	0.61
	162	-.060	2.8	46.6	3.5	0.35
	151	-.147	4.1	28.1	6.6	0.51
	134	-.159	4.4	27.6	7.0	0.55
	123	-.115	3.5	30.6	5.4	0.44
	110	-.085	3.1	36.2	4.3	0.39
	89	-.109	3.2	29.7	5.0	0.40

$\frac{di_R}{dV}$ = Residual Current Slope

I_o = Residual Drift Current

J_o = Integral Electron Flux ($E \gtrsim 15$ ev)

α = 1

CHAPTER V

DISCUSSION OF THE EXPERIMENTAL RESULTS

A. Introduction

The primary objective of this dissertation is to present experimentally determined electron energy distributions in the range of energies between approximately 0 and 15 ev. The results from the analysis of the current-voltage characteristics obtained with the pulse probe in the DC mode of operation were given in the two preceding chapters. No attempt will be made here to develop a theoretical model such that comparisons can be made with the measured distributions. This has been due in part to a lack of detailed experimental information concerning the cross-sections on various types of interactions.

In the first part of this chapter, we shall attempt to define briefly the type of interactions that might be considered as important and indicate as to where the experimental data is found to be most wanting in this regard. We shall restrict our discussion to only particle-particle interactions and review some of the past work regarding photoionization as the major source of generating primary electrons.

In the latter part of this chapter, we shall summarize some of our experimental results from the pulse probe and draw a few general conclusions concerning the experiment.

B. The Equilibrium Energy Distributions of Suprathermal Electrons

By the term "suprathermal electrons " we have meant electrons with energies greater than approximately 1 ev, without any particular reference to their source of origin, but set apart from the thermal electron gas.

If the production and energy loss of suprathermal electrons can be assumed to occur locally, the condition for equilibrium may be written as:

$$q(E)dE = F(E)\frac{dE}{dt}\bigg|_{E} - F(E)\frac{dE}{dt}\bigg|_{E + dE} = -d\left(F(E)\frac{dE}{dt}\right) \qquad (5.1)$$

or,

$$F(E) = \frac{\displaystyle\int_{E}^{\infty} q(E')dE'}{\dfrac{dE}{dt}}, \qquad (5.2)$$

where $F(E)dE$ is the number of electrons with energies between E and $E + dE$, per unit volume, $q(E)dE$ is the total production rate of electrons in the energy interval E and $E + dE$, per unit volume, and $\frac{dE}{dt}$ is the energy loss rate of the electrons. Equation (5.1) requires that the rate of production of electrons with energies between E and $E + dE$ be equal to the difference in the rates at which electrons leave and enter this energy interval as a result of various types of energy losses, such as from collisions with other particles.

Hanson (1963) has indicated that for altitudes below approximately 300 km the production and energy loss of fast electrons can be assumed to take place locally. In this section, we shall briefly review some of the work that has already been underway on the subject of photo-ionization and its relation to equation (5.2).

1. Production of Suprathermal Electrons

As the incident solar radiation penetrates the earth's atmosphere, its intensity is diminished by its interactions with the atmospheric constituents, such as scattering and absorption. When the

photon energy exceeds the ionization potential of a particular atom or molecule, photoionization may occur leading to the production of photoelectrons. Hinteregger, et al. (1965) have performed calculations for the primary photoionization rates of N_2^+, O^+, and O_2^+, as a function of altitude between approximately 90 and 350 km. The results show a maximum for the total primary production rate in the region of $\sim$ 140 km with a value of approximately 6×10^3 ions/cm^3-sec.

Dalgarno, et al. (1963), Hoegy, et al. (1965), and Shea, et al. (1968) have given results of calculations for the primary photoelectron production rates as a function of photoelectron energy for different altitudes. Their results indicate that at approximately 120 km there exists practically no primary photoelectrons produced in the 10 - 40 ev energy interval. The majority of the photoelectrons being produced have energies between 60 and 120 ev. Above approximately 150 km, the production spectrum is dominated by photoelectrons produced in the energy interval of 25 - 35 ev. (These values should only be considered as representative because of the many uncertainties in the cross-section data).

When the ejected primary photoelectron has a kinetic energy greater than the ionization potentials of the atoms or molecules it encounters, impact ionizations may occur, leading to the production of secondary electrons. These secondaries that are produced may contribute substantially to the total electron production function particularly for short wavelength photoionizations where the primary photoelectrons may possess sufficient energies to produce many secondaries.

Another possible process for the production of suprathermal electrons is from superelastic collisions where electrons are raised

from the thermal gas through interactions with either ions or neutrals that are in excited or metastable states. It is generally assumed that the secondaries (we shall use this term to mean all suprathermal electrons with the exception of the primary photoelectrons) have relatively low energies (less than approximately 10 ev) so that ionizations generated by secondaries are negligible.

If we assume that photoionization is the dominant source of primary suprathermal electron production, then we may write for the total production rate as:

$$q = q_p + q_s \quad ,$$

where q_p and q_s are the production rates of primary photoelectrons and secondary electrons, respectively, with $q \sim q_p$ at high energies ($E \gtrsim 10$ ev).

Thus, one would expect that at high energies the suprathermal energy distribution should be approximately the equilibrium primary photoelectron distribution. Hoegy, et al. (1965), Nagy and Fournier (1965), and Shea, et al. (1968) have performed the calculations for the equilibrium energy distributions of photoelectrons, using the solar flux data provided by Hinteregger (1965). We shall have occasion to discuss them in Section C of this chapter. Calculations for q_s, as a function of the energies of the secondaries, have remained a rather difficult problem and up to the present time have not been completely investigated.

2. Energy Loss Mechanisms

Hanson and Johnson (1961), Hanson (1963), and Dalgarno, et al. (1963) have discussed the various energy loss rates for fast electrons of different energies at different altitude regions. They have concluded that for electrons with energies above ~ 20 ev, the dominant energy loss

processes are through impact ionizations and allowed excitations of the neutral particles. The loss rate decreases with increasing altitude and the asymmetric energy variation of the loss rate shows a relatively broad maximum which peaks around 100 ev. Electronic excitation of the neutral particles was assumed to represent the major source of energy loss for electrons with energies in the range of 7 - 20 ev. This loss rate again decreases with increasing altitude and the energy dependence monotonically increases with the increasing of the electron energy. Due to the lack of experimental data on the many cross-sections for the various interactions, the analysis must necessarily be considered somewhat arbitrary.

In the energy interval of approximately 1.7 to 3.5 ev, the dominant energy loss mechanism was taken as vibrational excitation of N_2, particularly for the altitude region below approximately 200 km. The cross-section data for vibrational excitation of N_2 shows a maximum just below E $\sim$ 2.5 ev. Below approximately 1.7 ev, the energy losses are primarily through elastic collisions with the ambient electron gas and rotational excitation of N_2.

Elastic scattering of suprathermal electrons by neutral particles and positive ions are for the most part negligible because of the relative mass ratios. It is an important mechanism for the cooling of the thermal electrons because of the lack of other competing energy loss processes with the possible exception of rotational excitation of N_2. For the low energy suprathermal electrons (E $\lesssim$ 1.7ev) at low altitudes, the rotational excitation of N_2 may dominate depending on the thermal electron concentration. At high altitudes, greater than approximately

100 km, elastic scattering with the electron gas is probably the more
efficient process.

C. Review of the Experimental Results

1. The Secondary Distribution

The dominant contribution to the experimentally detected
secondary currents are from electrons with energies between approximately
1 and 8 ev. These currents were found to be exponential functions of
the retarding probe potentials with characteristic temperatures between
approximately 1 to 3 x $10^{4\,\circ}$K in the altitude region between $\sim$ 120 and
240 km. Detailed analysis of the forty current-voltage characteristics
indicate that the secondary energy distributions are devoid of any
"valleys" or "humps." There exists, for instance, no observable valley
between $\sim$ 2 to 4 ev that might be suggested by the energy losses as a
result from the vibrational excitations of N_2 (Hoegy, et al. 1965; Shea,
et al., 1968), just as there appears to be no hump near 5 to 6 ev as
might be expected from the simultaneous decrease of both vibrational and
electronic excitation energy losses.

Another competing energy loss process for the electrons in the
secondary distribution is through elastic collisions with the ambient
electron gas, particularly toward the low energy end and at high altitudes.
This process has been considered as the major source of selective thermal
heating of the electron gas, such that thermal electron temperatures exceed that
of the ion and neutral temperatures with the maximum deviation occurring in the
region near 200 km(Hanson & Johnson, 1961; Hanson, 1963; Dalgarno, et al.,1963).

When the energy losses from elastic collisions with the ambient
electron gas dominate, a formula for the energy loss rate may be expressed

as (Bulter and Buckingham, 1962):

$$\frac{dE}{dt} \sim \beta\ n_e\ E^{-\frac{1}{2}} \qquad (\frac{ev}{sec})\ , \qquad\qquad (5.3)$$

if the energies of the secondaries are much greater than the thermal

energies. The constant $\beta \sim 1.16 \times 10^{-4}$ in units of $ev^{3/2} - cm^3/sec$.

From the Druyvesteyn relationship as given by equation (2.18) and with

equation (5.2), it is readily seen that

$$\frac{d^2 i(V)}{dV^2} \propto \frac{1}{n_e} \int_{eV}^{\infty} q(E')dE'\ . \qquad\qquad (5.4)$$

If the rate of production of electrons is negligible for $E < E_a$,

then the contribution to the second derivative of the current from the

equilibrium distribution is a constant for the retarding probe potentials

$V < \frac{Ea}{e}$. Thus, the probe current becomes a quadratic function of the

retarding probe potential.

Theoretical considerations concerning the energy distributions

of the secondaries must begin with an examination of the relevant cross-

sections for the production of secondaries either from impact ionizations

or some other process such as superelastic collisions. Although some

experimental data is available with regards to impact ionizations by electrons

with energies just above or a few times the ionization potentials, such

as for N_2 (Field and Franklin, 1957 ; McDaniel, 1964), the variation of

q_s as a function of the energy of the secondaries requires further

investigation.

2. Electrons with Energies $\gtrsim$ 15 ev

The analysis of the residual probe current was performed in the

preceding chapter under the approximation that the electrons with energies greater than $\sim$ 15 ev possess a monoenergetic distribution. The derived quantities were n_o, the concentration for this high energy component, and $E_o = eV_o$ where V_o corresponds to the linear current intercept with the zero current axis. The results showed that the increases observed for the residual probe currents as the altitude increased were primarily due to the increasing of n_o with altitude (from $\sim$ 5 to 14 electrons/cm^3). The values for E_o, on the other hand, remained relatively constant ($\sim$ 26 ev) above approximately 160 km.

However, if we were to consider photoionization by the incident solar radiation as the dominant source of production of these electrons, the assumption of an equilibrium monoenergetic distribution can only be construed as a gross approximation. For an arbitrary high energy distribution function $f(E)$, it can be readily shown that the measured quantity E_o is related by:

$$E_o = \frac{\int_{E_1}^{E_2} f(E)E^{\frac{1}{2}}dE}{\int_{E_1}^{E_2} f(E)E^{-\frac{1}{2}}dE} \quad , \tag{5.5}$$

where $f(E)$ is normalized to unity and E_1, E_2 are the energy limits defining $f(E)$. Thus, E_o is a weighted average energy and can be related to the "range" of $f(E)$. (For instance, if we defined $K(E) = f(E)E^{-\frac{1}{2}}$ then,

$$E_o = \cfrac{\displaystyle\int_{E_1}^{E_2} K(E)E\ dE}{\displaystyle\int_{E_1}^{E_2} K(E)dE} \qquad).$$

As a case for illustration, consider an energy distribution function $f(E) \propto E^{-\frac{1}{2}}$, that is, a relatively slow decreasing function of energy and let us make some estimates for the value of $\Delta E = E_2 - E_1$. Since for this distribution function the expressions in equation (5.5) are easily integrated, it may be readily shown that if we take $E_1 \sim 20$ ev, we would get for $\Delta E \sim 12$ ev, with the average energy of the electrons for this distribution $\overline{E} \sim E_o \sim 26$ ev for the altitude region between approximately 160 to 240 km. Thus, we find that when we take a distribution function, which is a relatively slow function of energy, the distribution "range" is confined about E_o with the average energy near the value of E_o. If we had instead assumed this particular distribution function for the analysis of the residual probe current, the results for n_o, the concentration, would not be significantly different from the monoenergetic analysis.

D. Conclusions

The pulse probe operated in the DC mode has been shown to a large degree of success, capable of detection of both the thermal and the secondary electron distributions. The results of the thermal electron temperatures, as determined from the pulse probe measurements, can be compared with that obtained from the Langmuir probe experiment (Figure 5.1). The preliminary results indicate excellent agreement above approximately 160 km. At the present time, it is not clear why departures occur below
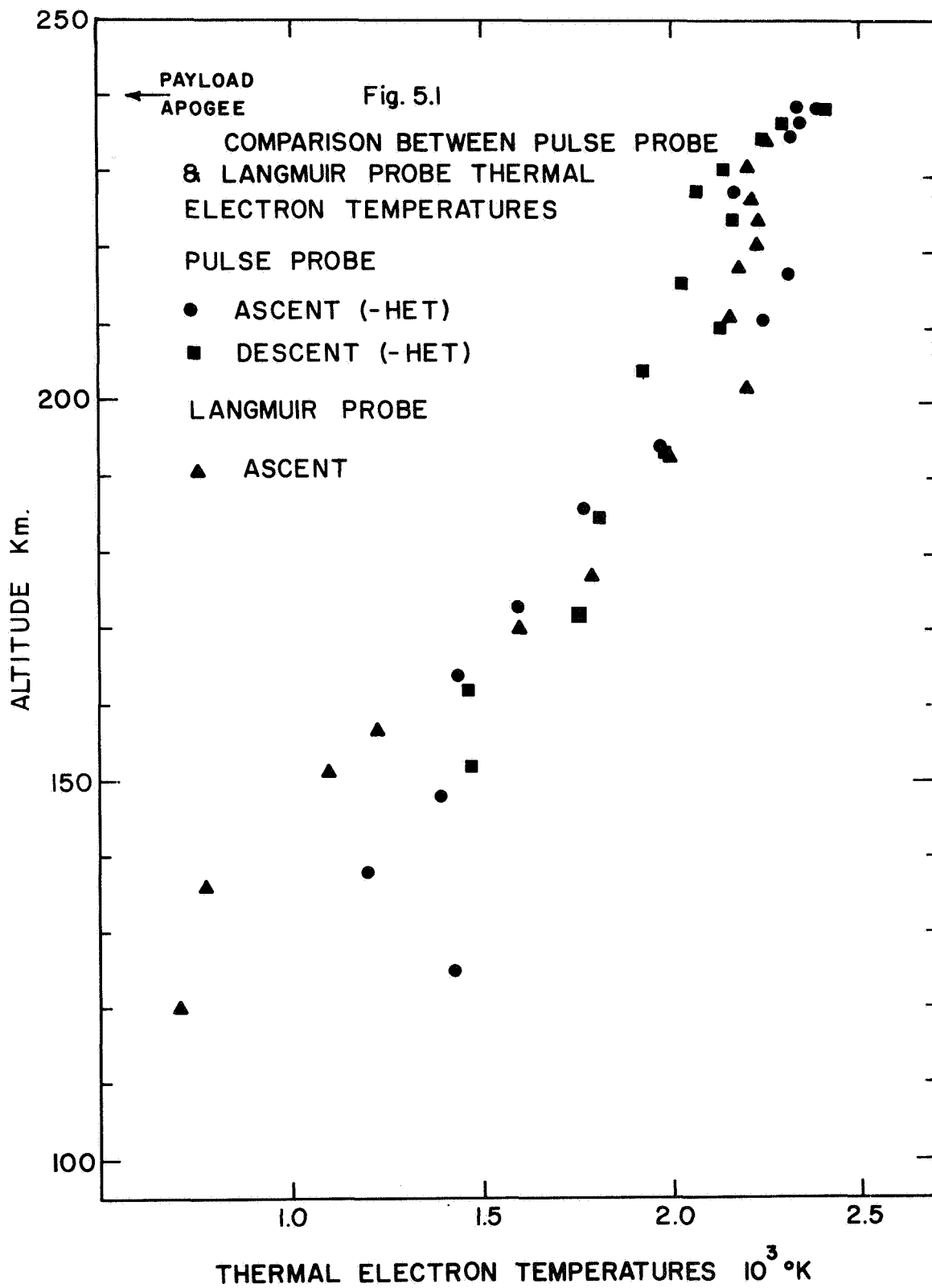
Fig. 5.1

COMPARISON BETWEEN PULSE PROBE
& LANGMUIR PROBE THERMAL
ELECTRON TEMPERATURES

PULSE PROBE

● ASCENT (-HET)

■ DESCENT (-HET)

LANGMUIR PROBE

▲ ASCENT

PAYLOAD APOGEE

ALTITUDE Km.

THERMAL ELECTRON TEMPERATURES 10^3 °K

Table 5.1 THERMAL AND SECONDARY ELECTRON TEMPERATURES

	Altitude (km)	$Tt(^oK)$	$Ts(^oK)$	$Tt'(^oK)$		Altitude (km)	$Tt(^oK)$	$Ts(^oK)$	$Tt'(^oK)$
Ascent	120		7,980		Descent	110		6,462	
	126	1,563	8,117	1,422		123		10,901	
	138	1,353	12,616	1,199		134		10,050	
	149	1,492	12,508	1,390		151	1,576	19,095	1,468
	164	1,591	24,243	1,435		162	1,560	23,465	1,461
	174	1,685	23,308	1,594		171	1,901	22,484	1,757
	187	1,890	26,170	1,769		184	1,933	27,334	1,804
	194	2,100	26,767	1,978		193	2,113	31,318	1,979
	202		31,328			204	2,043	26,426	1,924
	211	2,371	30,553	2,239		210	2,253	27,170	2,123
	217	2,464	27,721	2,305		216	2,160	29,642	2,029
	224	2,395	25,607	2,222		223	2,301	32,143	2,159
	228	2,325	30,820	2,165		227	2,198	32,601	2,065
	231		27,907			231	2,294	33,074	2,136
	235	2,485	28,039	2,308		235	2,446	28,714	2,237
	237	2,517	29,261	2,338		237	2,474	28,241	2,291
	239	2,525	30,308	2,382		239	2,512	32,547	2,393
Apogee	239	2,528	31,796	2,328					

Nike-Tomahawk 18.12 March 30, 1967
DC Mode

Tt = thermal temperature

Ts = secondary temperature

Tt' = thermal temperature corrected for secondary distribution

this altitude.

In order to experimentally determine the electron energy
distribution beyond 15 ev, the retarding potential for the probe would
have to be increased possibly to the order of 40 to 50 volts, based
on the discussion in the preceding section. Increasing the retarding
probe potential would mean that the ambient positive ions would undergo
much greater acceleration together with an increase in the positive
sheath dimension associated with the probe. An alternative technique
would be to shield the probe sweep from the plasma by moving it to an
inner grid and perform the energy selection there. The cage would then
be operated at some fixed potential relative to the vehicle, preferably
negative with respect to the plasma so that the Druyvesteyn relationship
remain applicable. However, there would then be a suppression of the
thermal electron collection. Another possible improvement in detection
in the DC mode of operation might be to measure the second derivative
of the current with respect to the retarding probe potential electronically.

The pulse technique of measuring electron concentration has not as
yet received a thorough examination, although preliminary results have
been encouraging. Direct concentration measurements can, in principle,
be made for both the thermal and secondary distribution as a function of
the retarding probe potential.

Recent improvements in probe construction techniques have permitted
the utilization of spherical pulse probes (launched aboard 14.298 and
18.30), however, without appreciable reduction in their overall dimensions
or increases in probe transparency. Thus, the requirement that the
vehicles have large conductive areas in direct contact with the ambient
plasma for providing a stable potential reference continues to exist.

The thermal equalization probes are currently the only experimentally established method by which vehicle to plasma potential may be continuously monitored. Further investigations of these experiments as well as into other possible techniques are highly desirable (good data are available from the thermal equalization probes on the flights 14.164 and 14.298).

Aside from encountering mechanical failures, which in some cases were catastrophic, the overall performances from the instrumentation packages as well as the designs for the various probes have proved to be satisfactory. The experimental results from the pulse probe measurements indicate the following general conclusions:

1) The energy distributions of electrons with energies less than $\sim$ 15 ev indicate two distinct populations, the thermal electron gas and a secondary distribution, with characteristic temperatures of $\sim$ 1.5 to 2.5 x 10^{3} ^{o}K and 1 to 3 x 10^{4} ^{o}K, respectively, in the altitude region between approximately 120 to 240 km.

2) The experimentally measured retarded probe currents resulting from these two distributions are exponential functions of the retarding probe potential. In particular, valleys or humps in the secondary energy distributions in the energy range between $\sim$ 1 and 8 ev were not observed.

3) The electron concentrations for the secondary distribution were found to be approximately constant between 150 to 240 km with an approximate value of 150 - 200 electrons/cm^{3}.

4) A high energy component (electrons with E $\gtrsim$ 15 ev) in the electron distribution was found to have contributed to the retarded

probe current in the range of potentials between $\sim$ 8 and 15 volts

relative to the plasma. The slopes and magnitudes of the linear

residual probe currents suggest that they have characteristic energies

of $\sim$ 26 ev and concentrations between $\sim$ 5 and 14 electrons/cm^3.

        5) The vehicle potential measurements as determined from

the current-voltage characteristics indicate values between

approximately 2 and 2.5 volts negative with respect to the plasma.

        Since the inception of our ionospheric research program in

1959, the development of new and diverse probing techniques has

gradually improved. In light of the quality of the present available

data, we anticipate advances toward systematic experimental explorations

into various ionospheric conditions and an improved theoretical

understanding of ionospheric interactions.

REFERENCES CITED

A. C. Aikin and S. J. Bauer, Introduction to Space Sciences, Chapter III, edited by W. N. Hess, Gordon and Breach Science Publishers, 133 (1965)

R. T. Bettinger, "An In Situ Probe System for the Measurement of Ionospheric Parameters," Ph.D. Thesis, University of Maryland, Department of Physics and Astronomy Tech. Rep. No. 277 (1964)

R. T. Bettinger and E. H. Walker, "A Relationship for Plasma Sheaths About Langmuir Probes," Phys. Fluids, 8, 748 (1965)

R. T. Bettinger, "Offset Voltages of Langmuir Probes in the Ionosphere," Rev. of Sci. Instru., 36, 630 (1965)

R. T. Bettinger, Interactions of Space Vehicles with an Ionized Atmosphere, Part I, edited by S. F. Singer, Pergamon Press, 163 (1965)

R. T. Bettinger and A. A. Chen, "An End Effect Associated with Cylindrical Langmuir Probes Moving at Satellite Velocities," J. of Geophys. Res., 73 (7), 2513 (1968)

R. E. Bourdeau, "Ionospheric Research from Space Vehicles," Space Sci. Rev., 1, 683 (1963)

P. J. Bowen, R. L. F. Boyd, C. L. Henderson, and A. P. Willmore, "Measurement of Electron Temperature and Concentration from a Spacecraft," Proc. Roy. Soc. A, 281, 514 (1964)

S. T. Butler and M. J. Buckingham, "Energy Loss of a Fast Ion in a Plasma," Phys. Rev., 126 (1), 1 (1962)

A. Dalgarno, M. B. McElroy, and R. J. Moffett, "Electron Temperatures in the Ionosphere," Planet. Space Sci., 11, 463 (1963)

M. J. Druyvesteyn, "Der Niedervoltbogen," Z. Phys., 64, 790 (1930)

REFERENCES CITED
(Continued)

F. H. Field and J. L. Franklin, Electron Impact Phenomena, Academic Press, (1957)

W. B. Hanson and F. S. Johnson, "Electron Temperatures in the Ionosphere," Memoires Soc. R. Sc. Liege, 4, 390 (1961)

W. B. Hanson and D. D. McKibbin, "An Ion-Trap Measurement of the Ion Concentration Above the F_2 Peak," J. Geophys. Res., 66 (6), 1667 (1961)

W. B. Hanson, "Electron Temperatures in the Upper Atmosphere," Space Res., 3, 282 (1963)

K. K. Harris, G. W. Sharp, and W. C. Knudsen, "Ion Temperature and Relative Ion Composition Measurements from a Low-Altitude Polar-Orbiting Satellite," J. of Geophys. Res., 72 (23), 5939 (1967)

H. E. Hinteregger, "Combined Retarding Potential Analysis of Photoelectrons and Environmental Charged Particles Up to 234 km," Space Res., 1, 304 (1960)

H. E. Hinteregger, L. A. Hall, and G. Schmidtke, "Solar XUV Radiation and Neutral Particle Distribution in July 1963 Thermosphere," Space Res., 5, 1175 (1965)

W. R. Hoegy, J. P. Fournier, and E. G. Fontheim, "Photoelectron Energy Distribution in the F Region," J. of Geophys. Res., 70 (21), 5464 (1965)

F. T. Huang, "Ionospheric Parameters from Langmuir Probe Measurements," Ph.D. Thesis, University of Maryland, Department of Physics and Astronomy, To Be Published

REFERENCES CITED
(Continued)

W. C. Knudsen and G. W. Sharp, "Ion Temperatures Measured Around
a Dawn-Dusk-Auroral-Zone Satellite Orbit," J. of Geophys. Res., 72 (3),
1061 (1967)

W. C. Knudsen, "Geographic Distribution of F-Region Electrons with
About 10 ev Energy," J. of Geophys. Res., 73 (3), 841 (1968)

I. Langmuir and H. M. Mott-Smith, "Theory of Collectors in Gaseous
Discharges," Phys. Rev., 28 (4), 727 (1926)

E. W. McDaniel, Collision Phenomena in Ionized Gases, John Wiley,
172 (1964)

S. J. Moss and E. Hyman, "Minimum Variance Technique for the
Analysis of Ionospheric Data Acquired in Satellite Retarding Potential
Analyzer Experiment," J. of Geophys. Res., 73 (13), 4315 (1968)

A. F. Nagy and J. P. Fournier, "Calculated Zenith Intensity of the
Second Positive Band of Molecular Nitrogen," J. of Geophys. Res., 70 (23),
5981 (1965)

M. Nicolet and A. C. Aikin, "The Formation of the D Region of the
Ionosphere," J. of Geophys. Res., 65, 1469 (1960)

R. C. Sagalyn, M. Smiddy, and J. Wisnia, "Measurement and
Interpretation of Ion Density Distribution in the Daytime F Region,"
J. of Geophys. Res., 68 (1), 199 (1963)

M. F. Shea, R. D. Sharp, and M. B. McElroy, "Measurements and
Interpretation of Low-Energy Photoelectrons," J. of Geophys. Res., 73 (13),
4199 (1968)

REFERENCES CITED
(Continued)

L. G. Smith, "Rocket Observations of Sporadic E and Related Features in the E Region," Radio Sci., 1, 178 (1966)

L. G. Smith, L. H. Weeks, and P. J. McKinnon, "Rocket Observations of Electron Temperatures in the E Region," GCA Tech. Rep. No. 67-13-N, (1967)

N. W. Spencer, L. H. Brace, and G. R. Carignan, "Electron Temperature Evidence for Nonthermal Equilibrium in the Ionosphere," J. of Geophys. Res., 67, 157 (1962)

N. W. Spencer, L. H. Brace, G. R. Carignan, D. R. Taeusch, and H. Niemann, "Electron and Molecular Nitrogen Temperature and Density in the Thermosphere," J. of Geophys. REs., 70 (11), 2665 (1965)